



ASTRO-H Space X-ray Observatory White Paper

Stellar-Mass Black Holes

J. M. Miller (University of Michigan), S. Mineshige (Kyoto University), A. Kubota (Shibaura Inst. of Tech.),
S. Yamada (Tokyo Metropolitan University), F. Aharonian (MPI, Heidelberg),
C. Done (University of Durham), N. Kawai (Tokyo Institute of Technology),
K. Hayashida (Osaka University), R. Reis (University of Michigan), T. Mizuno (Hiroshima University),
H. Noda (RIKEN), Y. Ueda (Kyoto University), and M. Shidatsu (Kyoto University)
on behalf of the ASTRO-H Science Working Group

Abstract

Thanks to extensive observations with X-ray missions and facilities working in other wavelengths, as well as rapidly-advancing numerical simulations of accretion flows, our knowledge of astrophysical black holes has been remarkably enriched. Rapid progress has opened new areas of enquiry, including measurements of black hole spin, the properties and driving mechanisms of jets and disk winds, the impact of feedback into local environments, the origin of periodic and aperiodic X-ray variations, and the nature of super-Eddington accretion flows, among others. The goal of this White Paper is to illustrate how *ASTRO-H* can make dramatic progress in the study of astrophysical black holes, particularly the study of black hole X-ray binaries.

Complete list of the ASTRO-H Science Working Group

Tadayuki Takahashi^a, Kazuhisa Mitsuda^a, Richard Kelley^b, Felix Aharonian^c, Hiroki Akamatsu^d, Fumie Akimoto^e, Steve Allen^f, Naohisa Anabuki^g, Lorella Angelini^b, Keith Arnaud^b, Marc Audardⁱ, Hisamitsu Awaki^j, Aya Bamba^k, Marshall Bautz^l, Roger Blandford^f, Laura Brenneman^b, Greg Brown^m, Edward Cackettⁿ, Maria Chernyakova^c, Meng Chiao^b, Paolo Coppi^o, Elisa Costantini^d, Jelle de Plaa^d, Jan-Willem den Herder^d, Chris Done^p, Tadayasu Dotani^a, Ken Ebisawa^a, Megan Eckart^b, Teruaki Enoto^q, Yuichiro Ezoe^r, Andrew Fabianⁿ, Carlo Ferrignoⁱ, Adam Foster^s, Ryuichi Fujimoto^t, Yasushi Fukazawa^u, Stefan Funk^f, Akihiro Furuzawa^e, Massimiliano Galeazzi^v, Luigi Gallo^w, Poshak Gandhi^p, Matteo Guainazzi^x, Yoshito Haba^y, Kenji Hamaguchi^h, Isamu Hatsukade^z, Takayuki Hayashi^a, Katsuhiro Hayashi^a, Kiyoshi Hayashida^g, Junko Hiraga^{aa}, Ann Hornschemeier^b, Akio Hoshino^{ab}, John Hughes^{ac}, Una Hwang^{ad}, Ryo Iizuka^a, Yoshiyuki Inoue^a, Hajime Inoue^a, Kazunori Ishibashi^e, Manabu Ishida^a, Kumi Ishikawa^q, Yoshitaka Ishisaki^f, Masayuki Ito^{ae}, Naoko Iyomoto^{af}, Jelle Kaastra^d, Timothy Kallman^b, Tuneyoshi Kamae^f, Jun Kataoka^{ag}, Satoru Katsuda^a, Junichiro Katsuta^u, Madoka Kawaharada^a, Nobuyuki Kawai^{ah}, Dmitry Khangulyan^a, Caroline Kilbourne^b, Masashi Kimura^{ai}, Shunji Kitamoto^{ab}, Tetsu Kitayama^{aj}, Takayoshi Kohmura^{ak}, Motohide Kokubun^a, Saori Konami^r, Katsuji Koyama^{al}, Hans Krimm^b, Aya Kubota^{am}, Hideyo Kunieda^e, Stephanie LaMassa^o, Philippe Laurent^{an}, François Lebrun^{an}, Maurice Leutenegger^b, Olivier Limousin^{an}, Michael Loewenstein^b, Knox Long^{ao}, David Lumb^{ap}, Grzegorz Madejski^f, Yoshitomo Maeda^a, Kazuo Makishima^{aa}, Maxim Markevitch^b, Hironori Matsumoto^e, Kyoko Matsushita^{aq}, Dan McCammon^{af}, Brian McNamara^{as}, Jon Miller^{at}, Eric Miller^l, Shin Mineshige^{au}, Ikuyuki Mitsuishi^e, Takuya Miyazawa^e, Tsunefumi Mizuno^u, Koji Mori^z, Hideyuki Mori^e, Koji Mukai^b, Hiroshi Murakami^{av}, Toshio Murakami^t, Richard Mushotzky^h, Ryo Nagino^g, Takao Nakagawa^a, Hiroshi Nakajima^g, Takeshi Nakamori^{aw}, Shinya Nakashima^a, Kazuhiro Nakazawa^{aa}, Masayoshi Nobukawa^{al}, Hirofumi Noda^q, Masaharu Nomachi^{ax}, Steve O' Dell^{ay}, Hirokazu Odaka^a, Takaya Ohashi^r, Masanori Ohno^u, Takashi Okajima^b, Naomi Ota^{az}, Masanobu Ozaki^a, Frits Paerels^{ba}, Stéphane Paltaniⁱ, Arvind Parmar^x, Robert Petre^b, Ciro Pintoⁿ, Martin Pohlⁱ, F. Scott Porter^b, Katja Pottschmidt^b, Brian Ramsey^{ay}, Rubens Reis^{at}, Christopher Reynolds^h, Claudio Ricci^{au}, Helen Russellⁿ, Samar Safi-Harb^{bb}, Shinya Saito^a, Hiroaki Sameshima^a, Goro Sato^{ag}, Kosuke Sato^{aq}, Rie Sato^a, Makoto Sawada^k, Peter Serlemitsos^b, Hiromi Seta^{bc}, Aurora Simionescu^a, Randall Smith^s, Yang Soong^b, Łukasz Stawarz^a, Yasuharu Sugawara^{bd}, Satoshi Sugita^j, Andrew Szymkowiak^o, Hiroyasu Tajima^e, Hiromitsu Takahashi^u, Hiroaki Takahashi^g, Yoh Takei^a, Toru Tamagawa^q, Takayuki Tamura^a, Keisuke Tamura^e, Takaaki Tanaka^{al}, Yasuo Tanaka^a, Yasuyuki Tanaka^u, Makoto Tashiro^{bc}, Yuzuru Tawara^e, Yukikatsu Terada^{bc}, Yuichi Terashima^j, Francesco Tombesi^b, Hiroshi Tomida^{ai}, Yohko Tsuboi^{bd}, Masahiro Tsujimoto^a, Hiroshi Tsunemi^g, Takeshi Tsuru^{al}, Hiroyuki Uchida^{al}, Yasunobu Uchiyama^{ab}, Hideki Uchiyama^{be}, Yoshihiro Ueda^{au}, Shutaro Ueda^g, Shiro Ueno^{ai}, Shinichiro Uno^{bf}, Meg Urry^o, Eugenio Ursino^v, Cor de Vries^d, Shin Watanabe^a, Norbert Werner^f, Dan Wilkins^w, Shinya Yamada^r, Hiroya Yamaguchi^b, Kazutaka Yamaoka^e, Noriko Yamasaki^a, Makoto Yamauchi^z, Shigeo Yamauchi^{az}, Tahir Yaqoob^b, Yoichi Yatsu^{ah}, Daisuke Yonetoku^t, Atsumasa Yoshida^k, Takayuki Yuasa^q, Irina Zhuravleva^f, Abderahmen Zoghbi^h, and John ZuHone^b

^aInstitute of Space and Astronautical Science (ISAS), Japan Aerospace Exploration Agency (JAXA), Kanagawa 252-5210, Japan

^bNASA/Goddard Space Flight Center, MD 20771, USA

^cAstronomy and Astrophysics Section, Dublin Institute for Advanced Studies, Dublin 2, Ireland

^dSRON Netherlands Institute for Space Research, Utrecht, The Netherlands

^eDepartment of Physics, Nagoya University, Aichi 338-8570, Japan

^fKavli Institute for Particle Astrophysics and Cosmology, Stanford University, CA 94305, USA

^gDepartment of Earth and Space Science, Osaka University, Osaka 560-0043, Japan

^hDepartment of Astronomy, University of Maryland, MD 20742, USA

ⁱUniversité de Genève, Genève 4, Switzerland

^jDepartment of Physics, Ehime University, Ehime 790-8577, Japan

^kDepartment of Physics and Mathematics, Aoyama Gakuin University, Kanagawa 229-8558, Japan

^lKavli Institute for Astrophysics and Space Research, Massachusetts Institute of Technology, MA 02139, USA

^mLawrence Livermore National Laboratory, CA 94550, USA

ⁿInstitute of Astronomy, Cambridge University, CB3 0HA, UK

^oYale Center for Astronomy and Astrophysics, Yale University, CT 06520-8121, USA

^pDepartment of Physics, University of Durham, DH1 3LE, UK

^qRIKEN, Saitama 351-0198, Japan

^rDepartment of Physics, Tokyo Metropolitan University, Tokyo 192-0397, Japan

^sHarvard-Smithsonian Center for Astrophysics, MA 02138, USA

- ¹Faculty of Mathematics and Physics, Kanazawa University, Ishikawa 920-1192, Japan
- ^uDepartment of Physical Science, Hiroshima University, Hiroshima 739-8526, Japan
- ^vPhysics Department, University of Miami, FL 33124, USA
- ^wDepartment of Astronomy and Physics, Saint Mary's University, Nova Scotia B3H 3C3, Canada
- ^xEuropean Space Agency (ESA), European Space Astronomy Centre (ESAC), Madrid, Spain
- ^yDepartment of Physics and Astronomy, Aichi University of Education, Aichi 448-8543, Japan
- ^zDepartment of Applied Physics, University of Miyazaki, Miyazaki 889-2192, Japan
- ^{aa}Department of Physics, University of Tokyo, Tokyo 113-0033, Japan
- ^{ab}Department of Physics, Rikkyo University, Tokyo 171-8501, Japan
- ^{ac}Department of Physics and Astronomy, Rutgers University, NJ 08854-8019, USA
- ^{ad}Department of Physics and Astronomy, Johns Hopkins University, MD 21218, USA
- ^{ae}Faculty of Human Development, Kobe University, Hyogo 657-8501, Japan
- ^{af}Kyushu University, Fukuoka 819-0395, Japan
- ^{ag}Research Institute for Science and Engineering, Waseda University, Tokyo 169-8555, Japan
- ^{ah}Department of Physics, Tokyo Institute of Technology, Tokyo 152-8551, Japan
- ^{ai}Tsukuba Space Center (TKSC), Japan Aerospace Exploration Agency (JAXA), Ibaraki 305-8505, Japan
- ^{aj}Department of Physics, Toho University, Chiba 274-8510, Japan
- ^{ak}Department of Physics, Tokyo University of Science, Chiba 278-8510, Japan
- ^{al}Department of Physics, Kyoto University, Kyoto 606-8502, Japan
- ^{am}Department of Electronic Information Systems, Shibaura Institute of Technology, Saitama 337-8570, Japan
- ^{an}IRFU/Service d'Astrophysique, CEA Saclay, 91191 Gif-sur-Yvette Cedex, France
- ^{ao}Space Telescope Science Institute, MD 21218, USA
- ^{ap}European Space Agency (ESA), European Space Research and Technology Centre (ESTEC), 2200 AG Noordwijk, The Netherlands
- ^{aq}Department of Physics, Tokyo University of Science, Tokyo 162-8601, Japan
- ^{ar}Department of Physics, University of Wisconsin, WI 53706, USA
- ^{as}University of Waterloo, Ontario N2L 3G1, Canada
- ^{at}Department of Astronomy, University of Michigan, MI 48109, USA
- ^{au}Department of Astronomy, Kyoto University, Kyoto 606-8502, Japan
- ^{av}Department of Information Science, Faculty of Liberal Arts, Tohoku Gakuin University, Miyagi 981-3193, Japan
- ^{aw}Department of Physics, Faculty of Science, Yamagata University, Yamagata 990-8560, Japan
- ^{ax}Laboratory of Nuclear Studies, Osaka University, Osaka 560-0043, Japan
- ^{ay}NASA/Marshall Space Flight Center, AL 35812, USA
- ^{az}Department of Physics, Faculty of Science, Nara Women's University, Nara 630-8506, Japan
- ^{ba}Department of Astronomy, Columbia University, NY 10027, USA
- ^{bb}Department of Physics and Astronomy, University of Manitoba, MB R3T 2N2, Canada
- ^{bc}Department of Physics, Saitama University, Saitama 338-8570, Japan
- ^{bd}Department of Physics, Chuo University, Tokyo 112-8551, Japan
- ^{be}Science Education, Faculty of Education, Shizuoka University, Shizuoka 422-8529, Japan
- ^{bf}Faculty of Social and Information Sciences, Nihon Fukushi University, Aichi 475-0012, Japan

Contents

1	Introduction	5
2	Black hole spin	6
2.1	Current Black Hole Spin Measurements	6
2.2	Disk reflection spin measurements with <i>ASTRO-H</i>	8
2.3	Connections to jet production	9
3	Disk winds	10
3.1	Current picture based on <i>Chandra</i> , <i>XMM-Newton</i> , <i>Suzaku</i>	10
3.2	Wind Outflow Rates, Launching Sites, and Driving Mechanisms	11
3.2.1	Detecting Wind Circulation	14
3.2.2	Probing Dynamical Timescales	15
3.3	The Disk-Wind-Jet Connection	16
3.4	Connections to jets and winds in AGN	17
3.4.1	Detection of Multiple Ionization Zones	18
3.4.2	Do Ultra-Fast Outflows (UFOs) Span the Mass Scale?	18
4	Low-frequency variability	20
4.1	Links to accretion geometries	20
4.2	Low-frequency QPOs and Lense-Thirring precession	21
4.3	Shot noise studies	24
5	Accretion flow evolution	25
5.1	Explorations of the low/hard state with <i>ASTRO-H</i>	25
5.2	Tests of the hard X-ray corona with <i>ASTRO-H</i>	26
5.3	X-ray Continuum Emission	28
6	Super-Eddington Accretion	29
6.1	Current Ideas	29
6.2	SS 433 with <i>ASTRO-H</i>	30
6.3	Models for ULXs	32

1 Introduction

Black hole X-ray binaries are laboratories for the study of fundamental physics, including strong gravitation, the nature of gas accretion and ejection over many orders of magnitude in accretion rate, and feedback between black holes and their host environments. Though the known population of these sources in the Milky Way and Magellanic Clouds is much smaller than the population of massive black holes that power active galactic nuclei (AGN), the proximity of Galactic X-ray binaries enables very sensitive observations. Moreover, the short time scales intrinsic to X-ray binaries make it possible to study the evolution of accretion flows into distinct phases or “states” that may connect with and explain different AGN classes.

Studies of black hole X-ray binaries with current and recent missions, including, e.g., *RXTE*, *Chandra*, *XMM-Newton*, *Swift*, and *Suzaku*, have made enormous progress. Observations have begun to constrain the angular momenta or “spin” of some black holes (e.g. Miller et al., 2002, 2009; Hiemstra et al., 2011; Reis et al., 2009b, 2011, 2012b; Shafee et al., 2006; McClintock et al., 2006; Steiner et al., 2011), and to explore connections between accretion disks and jets (e.g. Fender et al., 2004). Some spectra have hinted at the very nature of disk accretion itself (e.g. Miller et al., 2006a, 2008), while others point to complexity or structure in hard X-ray coronae (e.g. Makishima et al., 2008). Ionized X-ray disk winds have been discovered; these winds may bear close analogy to the X-ray warm absorbers observed in Seyfert AGN (King et al., 2013). At the same time, robust detections of quasi-periodic oscillations have finally been obtained from massive black holes (Gierliński et al., 2008; Reis et al., 2012a). “Ultra-luminous” X-ray sources have been studied in some detail; some modeling suggests that ultra-luminous X-ray sources (ULXs) are examples super-Eddington accretion (e.g. Gladstone et al., 2009; Vierdayanti et al., 2006a), while others treatments suggest that a subset of the most extreme ULXs may harbor intermediate-mass black holes (e.g. Matsumoto et al., 2001; Strohmayer & Mushotzky, 2003; Farrell et al., 2009; Strohmayer & Mushotzky, 2009; Sutton et al., 2012).

It is particularly noteworthy that many of these advances have bridged the mass scale, revealing a host of phenomena to actually be present in both stellar-mass black holes and AGN. It is also fortuitous that much of this observational progress has happened concurrently with rapid advances in numerical simulations of accretion flows (e.g. Ohsuga & Mineshige, 2011; O’Neill et al., 2011; Schnittman et al., 2012; McKinney et al., 2012). In this sense, the last several years have been something of a golden moment in the study of black hole X-ray binaries. However, progress on both observational and theoretical fronts has opened new areas of enquiry, and highlighted the need to make further progress in some emerging and established areas. A necessarily incomplete list of developing questions might include:

- What is the distribution of stellar-mass black hole spin parameters?
- Can systematic errors associated with spin constraints be reduced?
- What are the processes by which disk winds and jets are powered?
- How much mass and energy do winds and jets carry away to which direction?
- What is the geometry of the hard X-ray corona, and what emission mechanisms power hard X-ray production?
- Which emission mechanisms dominate at low Eddington fraction?
- Is gas bound to black holes at very low Eddington fraction?
- How can we understand the origin of the complex X-ray variability?
- What does super-Eddington accretion look like?

In each of these cases, *ASTRO-H* (Takahashi et al., 2012) will be able to make progress or make revolutionary observations. Its bandpass, sensitivity, and instrument complement are well suited to addressing each of these problems. The impact of these advances will be registered in many distinct areas of astrophysics. The goal of this White Paper is to explain how the instrumentation aboard *ASTRO-H* - coupled with carefully-planned observations - can make dramatic progress in the study of black hole X-ray binaries in particular, and black hole accretion generally.

2 Black hole spin

2.1 Current Black Hole Spin Measurements

X-ray measurements of black hole spin amount to explorations of some of the most fundamental predictions of General Relativity. Indeed, X-ray measurements and sub-mm VLBI imaging (Doeleman et al., 2008, 2012) are currently the only two means of probing gravitation in the strong field limit, and the latter will only work in two cases (Sgr. A* and M87). Even binary radio pulsars are typically separated by large multiples of GM/c^2 ; in contrast, the accretion disk around a maximally-spinning "Kerr" black hole can extend to just $\sim GM/c^2$. Apart from revealing a fundamental physical theory, black hole spin measurements likely hold the keys to understanding the birth and evolution of black holes (Miller et al., 2011), and the processes by which relativistic jets are launched (Narayan & McClintock 2012; Steiner et al. 2013; however see Fender et al. 2010; Russell et al. 2013; King et al. 2013).

Affecting a large change to the spin of a black hole requires a doubling of its mass. The spin of a black hole can therefore reveal the nature of its formation and evolution. In the case of massive black holes in galaxy centers, the spin of the central black hole is determined by accretion and by mergers. In general, these processes likely work in opposite directions, with accretion increasing the spin of the hole, and black hole mergers reducing the spin as spin vectors are not typically aligned (see, e.g., Berti & Volonteri, 2008). In contrast, a stellar-mass black hole with a low-mass companion star cannot double its mass, and a high-mass companion does not live long enough for mass doubling (nor is it clear that the accretion is not chaotic). This means that the spin of stellar-mass black holes is a rare glimpse into the inner workings of supernovae and/or gamma-ray bursts (e.g. Gammie et al., 2004).

Studies of massive black holes - particularly those at the center of galaxy clusters - have shown that relativistic jets are able to strongly influence large scale structure (e.g. Fabian et al., 2006). The cavities blown by jets can be used as coarse bolometers to trace the power of the jet (e.g. Allen et al., 2006), which is otherwise difficult since radio luminosity is not a precise trace of jet power (e.g. Merloni & Heinz, 2007). The power requirements implied by most extreme cavities require tapping the spin energy of a near-maximal Kerr black hole with a very high mass (McNamara et al., 2009). Of course, this is consistent with the predictions of Blandford & Znajek (1977), who showed that black hole spin energy could be tapped to power jets through magnetic connections to the ergosphere. Note, however, that recent theoretical work points to the importance of magnetic flux, not just spin (Sikora & Begelman, 2013); moreover, a broad range of spins may be difficult to reproduce in current cosmological simulations (Volonteri et al., 2013). Again, though, the timescales natural to massive black holes can complicate efforts to connect jet power and spin, whereas stellar-mass black holes may enable an answer to the problem of jet production.

All current means of measuring the spin of a black hole actually measure the inner radius of the accretion disk. The measurements rely on the assumption that the disk is truncated at the innermost stable circular orbit, or ISCO, which is set by General Relativity and sensitive to the spin parameter of the black hole (see e.g. Bardeen et al., 1972). In practice, this amounts to an assumption that there is a marked contrast in the emissivity of the plunging gas within the ISCO, relative to gas on stable orbits in the disk outside of the ISCO. There is no observational means of testing this assumption, but the latest numerical simulations specifically aimed at examining this assumption (those that analyze a large ϕ angle and numerous orbital timescales) suggest that the assumption is robust as long as radiative cooling is efficient (Shafee et al., 2008; Noble et al., 2009; Reynolds & Fabian, 2008). The assumption of a disk that remains at the ISCO must break down at a low fraction of the Eddington luminosity (L_{Edd}). However, the exact Eddington fraction at which this occurs is not yet clear. Some results suggest that the disk remains close to the ISCO for $L \geq 0.001 L_{\text{Edd}}$ and recedes at lower luminosity (e.g. Tomsick et al., 2009; Reis et al., 2010, 2011), while other results suggest that the disk may recede at a higher Eddington fraction (e.g. Makishima et al., 2008; Takahashi et al., 2008; Shidatsu et al., 2011).

There are currently three viable means of constraining or measuring the spin parameter of a black hole: quasi-periodic oscillations (QPOs), thermal continuum emission from the disk, and atomic emission and absorption features due to disk reflection. The QPOs that are most likely to reveal spin are the so-called high-frequency QPOs ($\text{few} \times 100$ Hz, and sometimes seen in 2:3 frequency ratios, e.g. Strohmayer 2000). The detection

of such QPOs may be within the capability of the *ASTRO-H* HXI instrument, but their detection has relied upon high-cadence monitoring of an outburst and careful data screening. Such studies are really the domain of proposed future missions such as Athena+ and WF-MAXI. Another problem with the QPOs is that there are many different models that point to different radii and spin, and there is no consensus on which model is correct. For these reasons, QPOs lie beyond the scope of this White Paper. It may also be possible to constrain or measure black hole spin using X-ray polarization (e.g. Dovčiak et al., 2008; Schnittman & Krolik, 2009), but this technique has not yet been attempted, and it is also beyond the scope of this White Paper.

Measurements of spin using thermal continuum emission from the accretion disk have the advantage of utilizing a major component of the flux seen in stellar-mass black holes. Said differently, the potential signal is ample. When the distance, mass, and inner disk inclination to a source are known, and when applied in phases where the disk emission is strongly dominant over non-thermal emission, new models enable the measurement of the black hole spin parameter (see, Shafee et al., 2006; McClintock et al., 2006). In the past, measurements of distance have typically carried large fractional errors, but parallax techniques - made more powerful with sensitivity upgrades to radio telescopes such as MERLIN and the VLA - hold much promise (e.g. Miller-Jones et al., 2009). A remaining difficulty is that the inclination of the inner disk need not be the same as that of the outer disk, and the alignment timescale may be quite long (e.g. Maccarone, 2002). However, this too may be remedied with radio observations: in cases where jet emission may be resolved, the axis of the jet may be taken as normal to the plane of the inner disk (e.g. Hjellming & Rupen 1995). Last, continuum-derived spins rely on correctly encapsulating the effects of scattering in the disk atmosphere; currently, this is done using an overall multiplicative constant that corrects the disk flux and temperature (Shimura & Takahara, 1995; Merloni et al., 2000).

The basic theory of X-ray disk “reflection” was rapidly developed after the detection of a broad Fe K line in Cygnus X-1 that could potentially have originated in the inner disk (e.g. Barr et al. 1985; George & Fabian 1991; Magdziarz & Zdziarski 1995). A broad, sometimes skewed Fe line is merely the most distinctive part of a disk reflection spectrum that is now understood to likely include a forest of low-energy atomic emission lines, the Fe line, and the Compton back-scattering hump peaking in the 20-30 keV range (for reviews, see Reynolds & Nowak 2003; Miller 2007). The *ASCA* mission flew CCDs capable of handling modest fluxes, leading to the detection of skewed disk lines in many Seyfert AGN (Tanaka et al., 1995). It was not until CCDs (plus or minus gratings) capable of handling high count rates aboard *Chandra*, *XMM-Newton*, and *Suzaku* were flown that the prevalence of relativistic disk lines in stellar-mass black holes became clear. Arguably, the first strong constraint or measurement of black hole spin using disk reflection was obtained in 2002 with *XMM-Newton* (Miller et al., 2002). Such lines are now observed in neutron star X-ray binaries as well (e.g. Bhattacharyya & Strohmayer 2007; Cackett et al. 2008, 2010; Papitto et al. 2009).

Disk reflection occurs in the atmosphere of an accretion disk. Models typically assume either a constant gas density, or an atmosphere in vertical hydrostatic equilibrium (e.g. Nayakshin & Kallman 2001). Most models only include external irradiation, but at least one new model includes X-ray emission from the midplane (e.g. Ross & Fabian 2007). Observations do not appear to be sensitive to such variations (Reis et al., 2008); this may be consistent with a scenario in which magnetic pressure sets a constant gas density (Blaes et al., 2006) and renders midplane emission relatively unimportant. The observed reflection spectrum depends strongly on the ionization of the disk, enabling robust measurements of this parameter (this is a more careful treatment of the hardening factor that is also important when measuring spins via the disk continuum). Reflection models are calculated in the fluid frame and must be convolved with a relativistic smearing function to match observations. Smearing models are based on ray-tracing, and are fairly robust (Beckwith & Done, 2004). Indeed, these models are even able to measure the inclination of the inner disk owing to the strong influence of viewing angle on line profiles. The emissivity of the accretion disk, $J(r) \propto r^{-q}$, is important to measuring spin accurately, but this too can be measured using smearing models. New theoretical efforts appear to be making firm predictions concerning emissivity profiles (Wilkins & Fabian, 2012), and both quasar microlensing observations (e.g. Morgan et al., 2008; Chartas et al., 2009, 2012; Mosquera et al., 2013) and X-ray reverberation studies in Seyferts (e.g. Fabian et al., 2009, 2012; Zoghbi et al., 2012; Cackett et al., 2012) imply *very* compact black hole hard X-ray coronae through measurements of very short lag time scales.

ASTRO-H is arguably best-suited to improving the measurement of spin via disk reflection spectra. The largest advantage to this technique is that the measurement is a relative one: the *degree* to which Special Relativity (broadening lines and enhancing blue wings through beaming) and General Relativity (creating extended red wings as photons lose energy escaping from a very deep potential) shape the spectrum forms the basis of the measurement. Whereas the absolute flux of a spectral feature can be difficult to measure (since calibration enters), the width of an atomic line is arguably easier to measure. And whereas an absolute measurement requires the mass and distance of the black hole to be known in advance, the mass and distance to the black hole are not required for reflection-derived spins. A secondary advantage of disk reflection is that it is readily observed in both massive black holes and stellar-mass black holes, enabling comparisons across the mass scale.

Employing modest quality metrics, 14 stellar-mass black hole spins have been measured using relativistic disk reflection techniques, and 7 have been measured using the disk continuum (see Miller et al., 2009, 2011; McClintock et al., 2011). Although the number measured using each method is small, the peaks of the spin distributions from the independent techniques agree and point to high spin. The fact that independent methods with partially independent systematics are arriving at a commensurate peak spin value may point to a situation where astrophysics dominates over systematic errors. Taken literally, and when compared to the implied natal spins of neutron stars, these results imply that stellar-mass black holes could be born in gamma-ray bursts rather than in typical supernovae (Miller et al., 2011). Of course, more spin measurements are urgently required in order to increase the statistics in each distribution, and to better sample the wings of each distribution.

Currently, there is no compelling evidence in favor of black hole spin as the source of jet power, though the utility of stellar-mass black holes for such purposes is increasingly clear. Claims of a correlation between spin and jet power have been made Narayan & McClintock (2012), but these appear to be statistically insignificant, and/or at least partially driven by data selection (Russell et al., 2013). Weak correlations, with slightly better statistical significance, may be found when comparing spin and jet power across the black hole mass scale (King et al. 2013). Here especially, additional spin measurements will drive future progress.

ASTRO-H will be able to advance studies of black hole spin in the following ways:

- The mission should be able to obtain excellent broad-band spectra of 1-2 transients per year. Particularly if observations are made both in the "high/soft" state (in order to utilize the disk continuum) and bright phases of harder states (in order to utilize disk reflection), it will be possible to measure 1-2 spins per year. In five years, then, *ASTRO-H* should gather 5-10 spin values, or 10-20 spins over 10 years of mission operation. *Thus, it is likely that ASTRO-H can double the current number of spin measurements.*
- For both the disk continuum and disk reflection, intervening disk winds can pose serious complications. A strong wind can alter the implied mass accretion rate, which is important to continuum measurements. It can also distort the shape of the continuum, which is important to both continuum and reflection techniques. The sensitivity of the SXS will permit the detection and characterization of even very weak absorption lines from a disk wind, and enable continuum and reflection components to be measured accurately.
- The extraordinary sensitivity and bandpass of the HXI will permit unprecedented studies of the hard X-ray continuum. This owes partly to the fact that the HXI sits behind a focusing hard X-ray telescope, and partly to innovative background rejection techniques. The HXI will facilitate the detection of even weak hard X-ray components, enabling better separation of the disk flux for continuum-based spin measurements. The improvements for reflection-based spins are likely to be at least as marked: the Compton back-scattering hump will be revealed extremely well using the HXI, enabling improved broad-band modeling.

2.2 Disk reflection spin measurements with *ASTRO-H*

A typical 100 ks observation of a black hole binary similar to MAXI J1836–194 in the "intermediate" state (Reis et al. 2012) will reveal a relativistic line and Compton hump in a manner that has yet to be seen with current observatories (see Figure 1). The unprecedented sensitivity of the SXS in energies up to and beyond the iron line region (4–8 keV), together with the overlap with the HXI will provide strong constraints on the inclination and emissivity of the accretion disk as well and on the black hole spin, as these parameters are

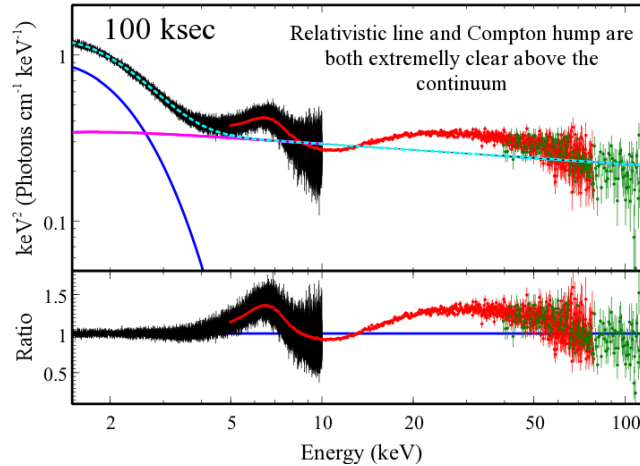


Figure 1: The presence of relativistic features including the broad Fe line and Compton hump will be revealed in detail with *ASTRO-H*. (Top) Simulated 100 ks spectrum of MAXI J1836–194 assuming a full reflection model and subsequently fit with a simple continuum consisting of an absorbed power law (magenta) and a disk blackbody (blue). (Bottom) Simulated data-to-model ratio emphasising the excellent sensitivity and energy coverage provided by *ASTRO-H*.

strongly dependent on the overall shape of the iron line and absorption depth complex and on the strength of the Compton hump at ~ 30 keV. Simulations show that *ASTRO-H* will determine the inclination and emissivity profile of systems like MAXI J1836–194, with 90% errors less than 1% and 3% respectively. These strong constraints on the inclination and emissivity directly lead to precise spin measurements, with *statistical* errors of approximately 1% for spin $\gtrsim 0.9$ for a source like MAXI J1836–194, and approximately 5% for spins $\lesssim 0.5$ for sources such as XTE J1752–223. For comparison, the current 90% statistical errors on the spin of MAXI J1836–194 ($a \sim 0.9$) and XTE J1752–223 ($a \sim 0.5$), both obtained with *Suzaku*, are 3.5% and 35% respectively.

2.3 Connections to jet production

X-ray binaries are often treated as *thermal* sources, effectively transforming the gravitational energy of the compact object (a neutron star or a black hole) into thermal X-ray emission radiated away by the hot accretion plasma. However, since the discovery of compact Galactic sources with relativistic jets (dubbed as microquasars) the general view on the role of nonthermal processes in X-ray binaries has significantly changed. It is now recognized that non-thermal processes do play a non-negligible role in these accretion-driven objects. Approximately 20 per cent of the ~ 250 known X-ray binaries show synchrotron radio emission, and observations in recent years have revealed the presence of radio jets in several classes of X-ray binary sources (e.g. Fender 2001). The high brightness temperature and the polarization of the radio emission from X-ray binaries are indicators of the synchrotron origin of radiation. The non-thermal power of synchrotron jets (in the form of accelerated electrons and kinetic energy of the relativistic outflow) during strong radio flares could be comparable with, or even exceed, the thermal X-ray luminosity of the central compact object.

If the acceleration of electrons proceeds at a very high rate, the spectrum of synchrotron radiation of the jet can extend to the hard X-ray and soft γ -ray domain (Atoyan & Aharonian, 1999; Markoff et al., 2001). In addition, the high density photon fields supplied by the accretion disk and by the companion star, as well as produced by the jet itself, create favorable conditions for effective production of X- and γ -rays of inverse Compton origin inside the jet (Levinson & Blandford, 1996; Atoyan & Aharonian, 1999; Georganopoulos et al., 2002). Generally, this radiation is expected to have an episodic character associated with strong radio flares in objects like GRS 1915+105.

A large fraction of microquasars are associated with Galactic black hole X-ray binaries. The previous observations (OSSE and COMPTEL) show that the spectra of these highly variable objects, in particular GRS 1915+105 and Cyg X-1, extend to the domain of very hard X-rays and soft gamma-rays. For any reason-

able temperature of the accretion plasma, models of thermal Comptonization cannot explain the MeV radiation, even when one invokes the so-called bulk-motion Comptonization. To explain this excess, the so-called “hybrid thermal/non-thermal Comptonization” model has been proposed; it assumes that the radiation consists of two components – (i) the thermal Comptonization component with a conventional temperature of the accretion plasma $kT_e \sim 20 - 30$ keV and (ii) a nonthermal high energy component produced during the development of a linear pair cascade initiated by relativistic particles in the accretion plasma surrounding the black hole (for a review see Coppi 1999). This model requires existence of a relativistic electron population in the accretion plasma, resulting from either direct electron acceleration or pion-production processes in the two-temperature accretion disk with $T_i \sim 10^{12}$ K (Mahadevan & Quataert 1997).

An alternative site for production of hard X-rays and low energy gamma-rays could be the synchrotron jets. In particular, it has been proposed that the synchrotron emission of microquasars might extend to X-ray energies, either in the extended jet structure (Atoyan & Aharonian, 1999) or close to the base of the jet (Markoff et al., 2001). Recently, a significant contribution of the nonthermal X-ray emission to the total X-ray luminosity of Cyg X-3 has been suggested by Zdziarski et al. (2012), based on detection of gamma-rays by *Fermi* LAT and *AGILE*. Confirming the existence of a synchrotron X-ray component from the jets in microquasars will not only help to understand the acceleration mechanisms in these objects, but also add to an emerging picture of disk–jet coupling.

The most promising energy band for the extraction of the synchrotron component is the hard X-ray to the soft gamma-ray band, where the radiation from the accretion plasma is suppressed. The performance of *ASTRO-H* the HXI and SGD are suited to spectroscopic and temporal studies of the most prominent representatives of microquasars like GRS 1915+105, Cygnus X-1, and Cygnus X-3. A detection of polarization by the soft gamma-ray detectors would provide crucial test of the synchrotron origin of radiation. In this regard, one should mention the claim of detection of polarization of hard X-ray emission above 400 keV by *INTEGRAL* which can be explained only by synchrotron emission (Laurent et al., 2011).

3 Disk winds

3.1 Current picture based on *Chandra*, *XMM-Newton*, *Suzaku*

During the last decade, a growing number of X-ray binaries have been found to exhibit absorption lines from highly ionized elements (Church et al., 2005; Boirin et al., 2004, e.g.,). These systems range from microquasars such as GRO J1655–40 (Ueda et al., 1998; Yamaoka et al., 2001; Miller et al., 2006a), GRS 1915+105 (Kotani et al., 2000; Lee et al., 2002; Ueda et al., 2009), H 1743 – 322 (Miller et al., 2006b) and 4U 1630 – 47 (Kubota et al., 2007) to low-mass X-ray binaries such as GX 13+1 (Ueda et al., 2001; Sidoli et al., 2002), X 1658–298 (Sidoli et al., 2001) and X 1254–690 (Boirin & Parmar, 2003). Blue-shifts indicative of winds are especially prominent in the black hole systems. In all cases, the sources are viewed at high inclination angles, and the absorption structure is visible throughout the orbital period (e.g., Yamaoka et al., 2001; Sidoli et al., 2001, 2002). The absorption features are therefore thought to originate in material that is associated with and extends above the accretion disk. This is illuminated by the X-rays produced from the innermost regions of the accretion flow (both the disk and hard X-ray coronal emission). The reprocessed emission and scattered flux from the extended wind can be seen directly in the “accretion disk corona” (or, ADC) sources, wherein the intrinsic X-rays are obscured (e.g. Kallman et al., 2003), but for the majority of highly inclined sources, the wind material is seen in absorption against the much brighter X-ray central engine. Multiple absorption lines give an excellent probe of the physical conditions in the wind (e.g., Ueda et al., 2004; Miller et al., 2006a), where the spectra indicate the presence of significant columns of highly-ionized outflowing material.

Several scenarios have been proposed to explain how winds are driven. One of the candidates is the radiation pressure on electrons. This can be made much more efficient if the cross section for interaction between the matter and radiation is enhanced by line opacity. There are multiple line transitions in the UV region of the spectrum, so UV emitting disks can drive a powerful wind at luminosities below Eddington. Such line–driven disk winds are seen in cataclysmic variables (CVs; (Pereyra et al., 2000)) and are probably also responsible for

the broad absorption line (BAL) outflows seen in AGN (Proga et al., 2000; Nomura et al., 2013). However, the disk temperature for black hole binaries is in the X-ray region, so line driving is probably unimportant (Proga & Kallman, 2002). The momentum absorbed in these observed transitions is very small, and insufficient to drive a wind.

Another type of outflow from a disk is a thermally-driven wind (Begelman et al., 1983). Here again, the central illumination is important, but the process is less direct. The illumination heats the upper layers of the disk to a temperature of order the Compton temperature, T_C . The atmosphere will expand due to the pressure gradient; at sufficiently large radii, the thermal energy driving the expansion is larger than the binding energy, leading to a wind being driven from the outer disk. Simple estimates of the launching radius of this wind give $R = 10^{12} \cdot (M/10M_\odot) \cdot (T_C/10^7 \text{ K})^{-1} \text{ cm}$ (Begelman et al., 1983). A separate analysis found that thermal winds can potentially be launched at a radius a factor 5–10 smaller than this (Begelman et al., 1983; Woods et al., 1996). *Chandra* grating data of GRS 1915 + 105 and *Suzaku* spectra of 4U 1630–47 (Kubota et al. 2007) may be consistent with a thermally driven wind: the data indicate a launching radius of $R \sim 10^{11} \text{ cm}$ (Ueda et al., 2009).

The last type of outflow is a magnetically-driven wind. These are much harder to quantitatively study as the magnetic field configuration is not known, yet they are almost certainly present at some level as the underlying angular momentum transport is known to be due to magnetic fields (see e.g. Balbus & Hawley, 2002). Winds (and jets) are clearly present in magnetohydrodynamical (MHD) simulations which include these magnetic stresses self-consistently. These generically show that the mass loss is stochastic, with large fluctuations both spatially and temporally, but that the time averaged properties are well defined, so this magnetic wind is quasi-continuous (e.g., Hawley & Krolik, 2001; Machida et al., 2004). These calculations are still in their infancy, especially for describing the properties of a geometrically-thin disk. An approximation to the properties of the self-consistent magnetic wind from an accretion disk can be made by imposing an external field geometry (Proga et al., 2000; Proga, 2003). The mass loss rates depend on this field configuration, but in general these allow steady, powerful winds to be launched from any radius. Similarly, imposing poloidal field lines in the disk can give rise to magnetocentrifugal winds (Blandford & Payne, 1982). Such winds transport angular momentum from the disk without the aid of internal viscosity, and they are known to exist in FU Orionis and T Tauri stellar systems based on evidence of rotation in absorption line profiles (Calvet et al., 1993).

A very small launching radius was obtained from *Chandra* grating spectra of GRO J1655–40 ($r \sim 10^{8-10} \text{ cm}$); this wind may be driven by magnetic pressure or via magnetocentrifugal acceleration (Miller et al., 2006a). This small launching radius was derived partly through the detection of density-sensitive Fe XXII lines, allowing for an accurate determination of the radius via $r = \sqrt{L/n\xi}$ (where L is the ionizing luminosity, n is the number density, and ξ is the ionization parameter). The observed absorption spectrum was later analyzed using a number of photoionization models constructed using Cloudy (Ferland et al., 1998) and XSTAR (Kallman & McCray, 1982); these models confirm a very small launching radius, and a very large mass outflow rate (Miller et al., 2008; Kallman et al., 2009). Even newer, more detailed treatments of thermal wind properties show that they cannot account for the wind in GRO J1655–40, again signaling a magnetic component (Luketic et al., 2010).

3.2 Wind Outflow Rates, Launching Sites, and Driving Mechanisms

X-ray gratings spectroscopy has revolutionized the study of black hole accretion. In particular, the resolution afforded by the *Chandra*/HETG and the *XMM-Newton*/RGS has made it possible to detect blue shifts in highly ionized X-ray absorption spectra, signaling the presence of disk winds in stellar-mass black holes. The consequences of winds can be far-reaching:

- Winds may remove angular momentum from the accreting gas, potentially enabling the basic operation of the accretion disk. Disk winds may hold the key to understanding the physics of disk accretion itself.
- Winds may remove more gas from a system than actually accretes onto the black hole, affecting both the growth of the black hole, and the evolution of the binary system.

- It is not yet clear if a single mechanism drives winds or dominates wind production, if different mechanisms may work at different times, or if multiple mechanisms may work concurrently. Detecting multiple ionization zones, constraining launching radii, and accurate measurements of total outflow rates can potentially reveal the answers.
- Stellar-mass black hole winds may be closely related to X-ray warm absorbers in Seyfert AGN, but the relationship is not yet clear.
- Wind and jets appear to be state-dependent; the disk may alternate its outflow mode. The nature of this phenomenon – and the clues it may provide to the physics of jet and wind production – remain to be discovered.

Spectroscopy of black hole X-ray binary winds with the *ASTRO-H*/SXS calorimeter will offer some clear advantages compared to dispersive spectrometers. Most important, perhaps, are the significant gains in resolution in the Fe K band. The baseline resolution of the SXS is just 5 eV, and this is fixed across its bandpass. Unlike a grating instrument, then, *the resolution of a calorimeter improves with increasing energy*. Whereas current instruments excel at detecting lines such as Fe XXV He- α and Fe XXVI Ly- α , the SXS will also do an excellent job of detecting their associated β lines, He-like and H-like Ni lines, and any lines or edges that are significantly blue-shifted. As a result, *ASTRO-H* will be sensitive to the most powerful components of outflows, and do a superior job of revealing the power in wind feedback from black holes into their local environments.

In this white paper, we have conducted a number of simulations to demonstrate the potential of *ASTRO-H*, and particularly the SXS, to greatly improve our view of accretion onto black holes. In these efforts, we have assumed a baseline calorimeter resolution of 5 eV. It is also important for the reader to note that a tunable onboard X-ray source will periodically be used to calibrate and measure the performance of the SXS. This means that the incredible intrinsic resolution of the calorimeter to measure small velocity shifts will be fully realized.

The mass outflow rate in a wind is given by:

$$\dot{M}_{wind} = \Omega C_v \mu m_p n_e r^2 v \quad (1)$$

where Ω is the covering factor ($0 \leq \Omega \leq 4\pi$), C_v is the filling factor, μ is the mean atomic weight (usually $\mu = 1.23$), m_p is the proton mass, n_e is the electron number density, r is the distance from the source of ionizing flux to the detected absorption zone, and v is the observed outflow velocity.

Stellar-mass black hole winds may represent a simpler environment than X-ray “warm absorber” winds in Seyfert AGN. For instance, optical and infrared constraints on the binary inclination and comparisons of emission and absorption lines strongly suggest *equatorial* winds, so Ω is fairly well constrained ($\Omega = 0.3 - 0.5$ is reasonable, see Miller et al. 2008, Ueda et al. 2009). Stellar-mass black hole disk winds are very highly ionized, in general, and have not shown evidence of a low ionization component. Therefore, they are not likely to be clumpy, so $C_v = 1$ is reasonable. As noted above, the resolution of the SXS will enable extremely accurate measurements of the observed wind velocity v . Of course, the observed velocity v is effectively a lower limit, since a vertically-launched wind will only have a component of its velocity along an equatorial line of sight, and any disk wind that retains its local Keplerian velocity will automatically be within $\sqrt{2}$ of its local escape velocity.

Although He-like triplets can provide useful density diagnostics, these features can arise whenever gas is illuminated; such lines are not necessarily tied to the disk wind. Recently, it has been shown that Fe XXII absorption lines at 11.92 Å and 11.77 Å (1.040 keV and 1.053 keV, respectively) can act as direct diagnostics of the wind density (Miller et al. 2006, 2008; King et al. 2012a; also see Mauche & Raymond 2000). At this energy, the resolution of the SXS is lower than that of the *Chandra*/HETG. Can the SXS confidently detect and resolve such lines?

To answer this question, we have simulated an 100 ks SXS spectrum, using the best-fit broadband XSTAR photoionization model of GRO J1655–40 (Miller et al. 2008) as a template. This source was observed at a flux of 1 Crab, which will give approximately 2000 counts/s in the SXS. After silencing the central 5 pixels

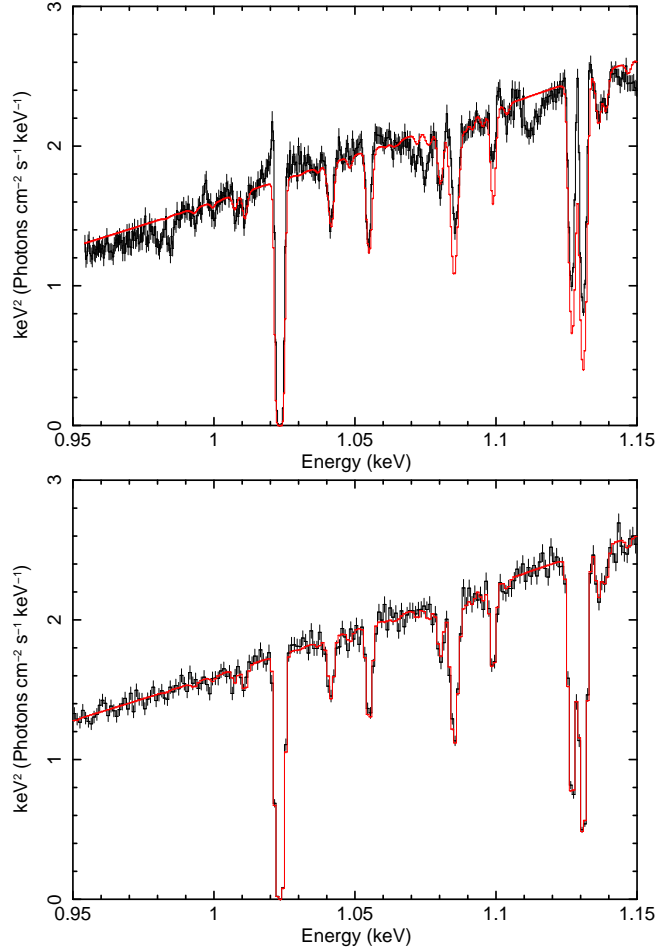


Figure 2: Top: The *Chandra*/HETG spectrum of GRO J1655–40 is shown here. The Fe XXII lines at 1.040 keV and 1.053 keV are clearly detected, and their flux ratio gives a density of $n = 10^{14} \text{ cm}^{-3}$. Bottom: Although the resolution of the HETG is superior to the *ASTRO-H*/SXS at 1 keV, this simulated 100 ks SXS spectrum demonstrates that the density-sensitive Fe XXII pair can easily be detected and resolved using the SXS. (Both spectra were binned for visual clarity.)

in the array, the recorded high and medium count rate will be 60 counts/s. Figure 2 shows the observed *Chandra*/HETG spectrum of GRO J1655–40 and the simulated *ASTRO-H*/SXS spectrum. While the resolution of the HETG is better at 1 keV, the Fe XXII lines are clearly detected and resolved in the SXS spectrum.

This simulation should be regarded as a proof of principle, because the spectrum observed from GRO J1655–40 is atypically rich. However, when such density diagnostics are available, one can obtain a very strong constraint on the wind launching radius (since $r = \sqrt{L/n\xi}$). This is important because within the Compton radius, highly ionized winds can only be driven magnetically (Begelman, McKee, & Shields 1983; also see Miller et al. 2008, Kallman et al. 2009, Luketic et al. 2010)

In other cases – particularly for highly obscured sources – it may not be possible to detect the Fe XXII pair near to 1 keV. In this case, the capabilities of the calorimeter will again help to determine wind properties accurately. When n_e cannot be obtained directly, it is typical to assume that $N = n_e r$ (where N is the column density). Because the SXS can readily detect higher order lines from He-like and H-like Fe and Ni, it can assess the extent to which such absorption is saturated, and provide much stronger constraints on the column density of disk winds than has previously been possible. Even in the absence of a direct density constraint, the total mass outflow rate may still be estimated via:

$$\dot{M}_{wind} = \Omega C_V \mu m_p L_{ion} v / \xi. \quad (2)$$

Here again, the ability of the SXS to measure v is important, but so too is the broad bandpass of *ASTRO-H*, and the sensitivity of the HXI. Since Fe XXV and Fe XXVI are ionized by X-rays above 8.8 keV and 9.3 keV, respectively, it is important to know the continuum up to high energy in order to accurately estimate the outflow rate in the hottest part of the disk wind.

3.2.1 Detecting Wind Circulation

The radii from which winds are launched in FU Ori and T Tauri stellar systems are not large compared to the source of ionizing flux. In other words, local flux is able to imprint on local gas, and the observed absorption profiles show the hallmarks of a rotating disk wind (e.g Calvet, Hartmann, & Kenyon 1993). This strongly signals that the disk winds in these systems are driven through a magnetocentrifugal process, as described by Blandford & Payne (1982).

The magnetocentrifugal wind model was conceived as an answer to the question of how gas in a disk might lose angular momentum, and where the angular momentum must go, in the absence of a companion star and binary orbit that may act as a reservoir. Thus, it may be particularly important in stellar systems and in AGN. But in those cases, too, thermal disk spectra suggest that internal magnetic viscosity is also at work in transporting angular momentum. It is entirely possible that the mechanisms work jointly. Evidence of magnetically-driven winds is emerging in black holes such as NGC 4151 (Kraemer et al., 2005), GRO J1655–40 (Miller et al. 2006, 2008), NGC 4051 (King et al., 2011), and possibly also IGR J17091–3624 (King et al., 2012b) and H 1743–322 (Miller et al., 2006b). Circulation may not be a signature unique to magnetocentrifugal winds, but it is worth addressing the ability of the *ASTRO-H* to reveal circulation.

Let us assume that a wind is being launched through magnetocentrifugal acceleration, and that it is executing local Keplerian motion as it also flows radially. An observed line will have a net blue-shift owing to its velocity into our line of sight, but will have small variations about the net shift owing to orbital motion, of approximately $v \simeq v_{Kep} r_h / r_w$ assuming a small angle approximation (where r_h is the radius of the central engine producing the hard ionizing flux, and r_w is the radius from the central engine at which the wind is detected). The matter is particularly simple when scaled in gravitational radii since $v_{Kep} = c / \sqrt{w}$, where w is the number of gravitational radii. Then v_w is also at w radii, and we can scale r_h to be at hGM/c^2 as well. Finally, we expect symmetric wings about the line centroid of $v = \pm ch/w^{3/2}$.

The size of the hard X-ray corona is not known well, especially in soft states wherein disk winds are detected. Values of 10–100 GM/c^2 may be reasonable. Winds in sources such as GRO J1655–40 and H 1743–322 may originate as close as $r \simeq 10^9$ cm; this is of order 1000 GM/c^2 . Even for a coronal radius of just 10 GM/c^2 , we expect wings offset from the line centroid by $v = \pm 100$ km/s. This is an order of magnitude below the measured FWHM of the Fe XXV and Fe XXVI lines detected in stellar-mass black hole winds. Of course, if the corona has a typical radius of 50 GM/c^2 , then we expect wings offset by $v = \pm 500$ km/s, which agrees better with measured line widths.

As an example, we consider the rich absorption spectrum observed from GRS 1915+105 in a soft state at a flux of about 1 Crab, using the *Chandra*/HETG (Neilsen & Lee, 2009; Ueda et al., 2009). The Fe XXV He- α line has a FWHM of 1200–1900 km/s (Neilsen & Lee 2009). Figure 3 shows this spectrum; it is interesting to note that neither line profile appears to be exactly symmetric, but there is stronger evidence of structure in the Fe XXV line. The figure shows the Fe XXV and Fe XXVI lines fit with two Gaussians, as a simplified case of rotation-induced line profiles. The composite line profile is not clear at the resolution of the *Chandra*/HETG. Using this model, however, we simulated a 100 ks *ASTRO-H*/SXS spectrum. Again, at a flux of 1 Crab, we expect an incident count rate of 2000 counts/s, and an effective rate of 60 counts/s. Figure 3 also shows this simulated spectrum, and the composite nature of the line profile is extremely clear at SXS resolution.

This is a simplified treatment of the problem of detecting orbital motion through absorption spectra. It shows that plausible coronal sizes and wind launching radii may encode Keplerian motion that could potentially be detected. Realistic line profiles will not be as clear as the simplified two-Gaussian models used in this simulation. The differences in Keplerian orbital velocities over a range in radii will naturally give rise to a significant line width, and signatures of rotation will be an addition to this broadening, not an alternative. The

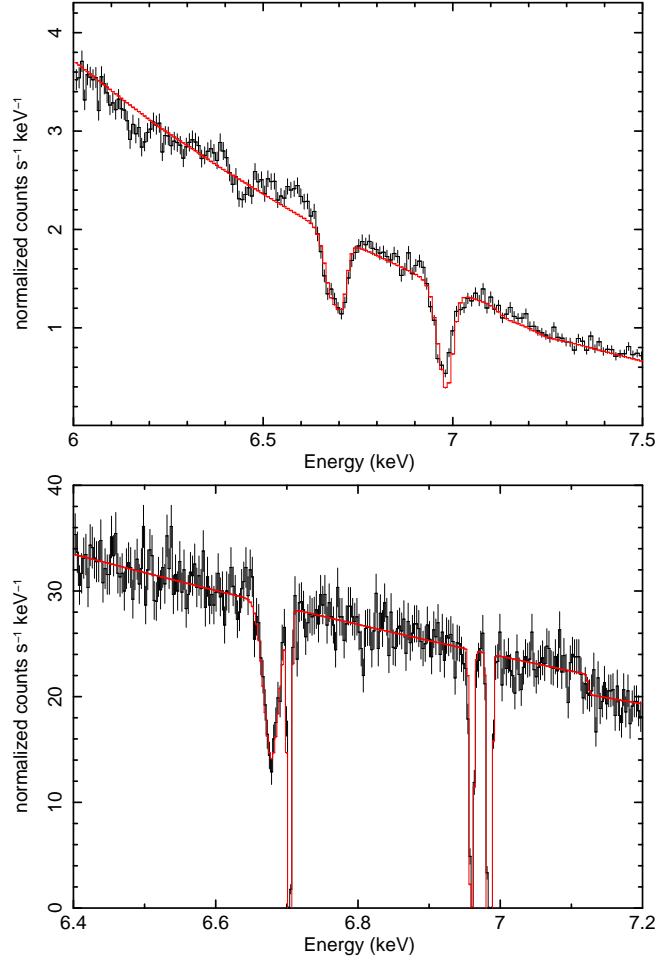


Figure 3: Top: A *Chandra*/HETG spectrum of GRS 1915+105 is shown here. The Fe XXV He- α and Fe XXVI Ly- α lines at 6.700 keV and 6.970 keV show some evidence of structure. The model shown in red fits each line with a composition of two Gaussians. Bottom: A simulated 100 ks *ASTRO-H*/SXS spectrum is shown here, generated using the model shown above. The SXS is clearly able to separate the individual components that are blended at lower resolution. Plausible size scales for the central engine, and the smallest wind launching radii that have been inferred, could give rise to spectra where rotation is encoded into absorption. This exercise shows that detecting a circulating, magnetocentrifugal wind is within the reach of the SXS.

chances of a detection are improved if $\delta r/r$ is small for a given wind. Moreover, it is possible that other factors may complicate the detection of orbital motion; for instance, the structure in the Fe XXV line in GRS 1915+105 may be due to the intercombination line being detected in absorption at very high density. Nevertheless, it appears that rotational motion is potentially within the grasp of *ASTRO-H*.

3.2.2 Probing Dynamical Timescales

The sensitivity and resolution of the SXS may make it possible to probe and utilize the dynamical timescale of winds in stellar-mass black holes, in order to better understand their origin. The dynamical timescale is simply given by $t_{dyn} = r/v_{out}$. Prior studies of GRO J1655–40 find that r is likely quite small, about 10^9 cm, with a characteristic outflow velocity of $v_{out} = 400$ km/s (Miller et al. 2008, Kallman et al. 2009), making $t_{dyn} \approx 25$ s. This time scale is likely too short to be probed with the SXS, even for sources as bright as 1 Crab.

However, other sources may offer different opportunities. The wind in GRS 1915+105 may be driven thermally from the outer disk. Neilsen et al. (2011) estimate that the wind originates at 46 light-seconds (1.4×10^{12} cm) from the black hole. For a characteristic outflow velocity of $v = 1000$ km/s, this gives $t_{dyn} = 13.8$ ks, which is fairly long.

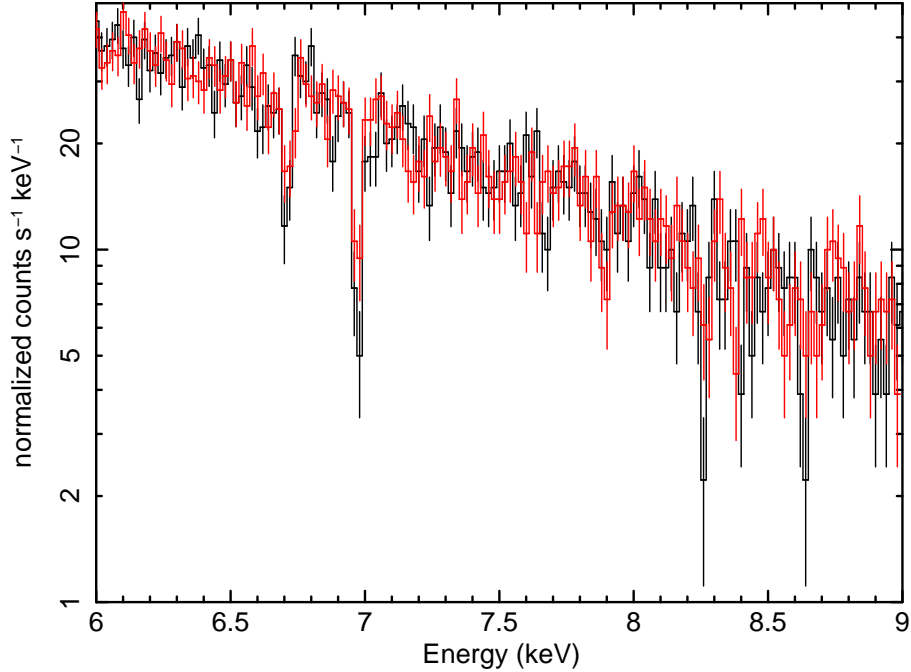


Figure 4: The plot above shows simulated 3 ks *ASTRO-H/SXS* spectra of GRS 1915+105, based on the *Chandra/HETG* spectrum shown in the previous figure. The spectrum in black has a 50% higher column density than the spectrum showing in red. Both spectra have been binned for visual clarity. For published values of the outflow velocity and launching radius of the wind in GRS 1915+105 (Neilsen & Lee 2009), 3 ks is well below the dynamical timescale in the wind ($t_{\text{dyn}} = r_{\text{wind}} / v_{\text{wind}}$). This simulation indicates that at least in the case of bright stellar-mass black holes with strong absorption spectra, dynamical timescales in the wind can be probed using the *ASTRO-H/SXS*.

Here again, we consider the line-rich wind absorption spectrum that was observed in GRS 1915+105 in a soft state at a flux of approximately 1 Crab. The spectrum is treated as "S1" in Neilsen & Lee (2009) and Ueda et al. (2009), and it is possible to model it with a single highly-ionized XSTAR absorption zone (e.g. King et al. 2013). This flux level will give ~ 2000 c/s in the SXS, or approximately 60 H+M c/s after silencing the central five pixels in the array.

Using the best-fit XSTAR photoionization grid in King et al. (2013), we simulated SXS spectra assuming the same column density measured in the *Chandra/HETG* spectrum ($1.1 \times 10^{23} \text{ cm}^{-2}$ in our fits), and half of that column density. Figure 4 shows that a 50% variation in the column density becomes visible in about 3 ks, which is shorter than the nominal dynamical time scale in the wind. This suggests that, at least in some sources, the SXS will be able to set upper limits on wind launching radii simply by detecting variations in e.g. column density or outflow velocity that exceed any variations in the source luminosity.

3.3 The Disk-Wind-Jet Connection

Compact, steady, relativistic jets are ubiquitous in the low/hard state of stellar-mass black holes (Fender et al., 2004). Sensitivity in the radio band has recently increased dramatically, and it is clear that jets are quenched in the disk-dominated high/soft states wherein winds are detected in stellar-mass black holes (Russell et al., 2011). But is the reverse true?

It appears that disk winds are state-dependent, and quenched in the low/hard state (Miller et al. 2006a, 2008; Neilsen & Lee 2009; Blum et al. 2010; King et al. 2012b; Ponti et al. 2012). This is particularly interesting because Seyfert AGN are radio-quiet and outflowing X-ray warm absorber winds are seen in these systems; however, warm absorbers are not observed in e.g. LLAGN, which can be radio-loud and bear a closer resemblance to the low/hard state. Recent work has also noted that the power in wind and jets may be regulated in a common way (King et al. 2013), potentially hinting at some common physics in their driving mechanisms.

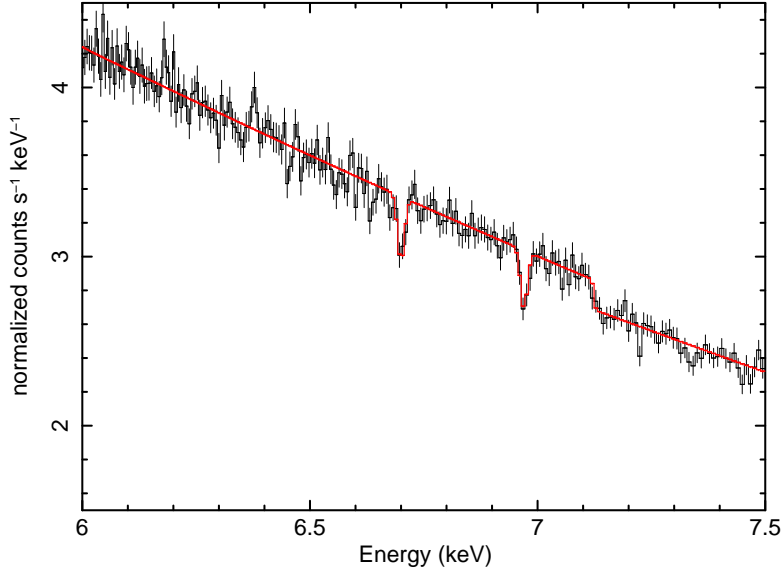


Figure 5: X-ray disk winds and relativistic radio jets in stellar-mass black holes are observed to be state-dependent: the accretion flow appears to alternate the outflow mode. This could point to a fundamental connection between the flows, and connections to the physical state of the inner disk. This is not easily explained in terms of thermal winds, and may require that winds have a strong magnetic component, as jets are suspected to have. Ruling out winds in the low/hard state, where jets are observed, is therefore very important. The plot above shows a simulated 200 ks *ASTRO-H*/SXS spectrum of a 0.1 Crab source in the low/hard state, assuming Fe XXV and Fe XXVI line equivalent width of just 2 eV, which is within current upper limits. Clearly, *ASTRO-H* can detect very weak disk winds that may persist in the low/hard state.

It is possible, though, that very fast, highly ionized winds with a low column density are hiding in the low/hard state. Such flows might be missed in a CCD spectrum with only moderate resolution, or even in a gratings spectrum. If such flows can be ruled-out, it would affirm that winds and jets are fundamentally anti-correlated. This would be particularly hard to reconcile with thermal driving models, because the outer disk should always be irradiated by the central engine, at least in the absence of an additional obscuring geometry.

To illustrate the power of *ASTRO-H* to address this science, Figure 5 shows a simulated 200 ks observation of a black hole in the low/hard state. The continuum spectrum and flux was taken from the deepest *Chandra*/HETG spectrum of H 1743–322 in that state, in which 90% confidence upper limits of just 2 eV are obtained for Fe XXV and Fe XXVI absorption lines. The same power-law continuum and absorbed flux (0.05 Crab, giving approximately 100 c/s and 50 H+M c/s in the SXS) was assumed, as well as line equivalent widths of just 2 eV. In 200 ks, these incredibly weak lines can be detected at the 5σ level of confidence. If winds persist in the low/hard state, even with a very low column density, they will be detected with *ASTRO-H*.

3.4 Connections to jets and winds in AGN

As noted previously, the advent of gratings spectroscopy made it possible to detect blue-shifted X-ray absorption in equatorial disk winds. Absorption of this sort is at least superficially similar to X-ray “warm absorbers” in Seyfert AGN. It is possible that there are fundamental connections between X-ray binary disk winds and Seyfert warm absorbers, and a number of questions immediately emerge: Are the outflows in both stellar-mass black holes and Seyfert AGN driven by the same process? Are they launched at the same radius (in a GM/c^2 sense)? An early comparison of winds across the mass scale suggests that the answer to these questions may be “yes” (King et al. 2013). However, this work also points to the need for improved observations, of exactly the sort that *ASTRO-H* can deliver.

3.4.1 Detection of Multiple Ionization Zones

X-ray “warm absorbers” in Seyferts consist of at least 2 – 3 ionization zones, although some authors adopt a continuous ionization gradient. It is particularly important to detect and measure the highest ionization components, since these appear to carry the most mass (Crenshaw & Kraemer, 2012; King et al., 2013). If massive black hole wind feedback into host galaxies is able to significantly affect galactic evolution, the most highly ionized wind components – which carry the bulk of the mass (Crenshaw & Kraemer 2012; King et al. 2013) – will have mattered the most. By virtue of its resolution and collecting area, *ASTRO-H* will be ideally able to detect highly ionized absorption in the Fe K band. Comparing these highly ionized components to the hot, ionized outflows observed in stellar-mass black holes will facilitate the most consistent comparisons of winds across the mass scale. This will greatly further attempts to understand if aspects of winds scale with mass in the way that jet properties appear to scale.

In comparing X-ray binaries and AGN, it becomes important to understand whether or not stellar-mass black hole winds are really described by a single absorption component. Even the most complex wind spectrum yet observed – that seen in GRO J1655-40 (Miller et al. 2006, 2008) – can be modeled fairly well using only one component. Modeling by Kallman et al. (2009) suggests that an improved fit is possible with an additional very highly ionized zone that is particularly prominent in the Fe K band. Moreover, recent spectroscopy of IGR J17091–3624 has also found evidence of two zones separated more in velocity than in ionization (King et al. 2012).

Figure 6 shows the *Chandra*/HETG data reported in Miller et al. (2006a, 2008) and Kallman et al. (2009). The data have been fit with a dominant absorption zone described by $\log(\xi) = 4.1$, $N_{\text{H}} = 3.0 \times 10^{23} \text{ cm}^{-2}$, and $v = 400 \text{ km/s}$, and by a second possible zone with $\log(\xi) = 6.0$, $N_{\text{H}} = 2.0 \times 10^{23} \text{ cm}^{-2}$, and $v = 1400 \text{ km/s}$ (Kallman et al. 2009). Scattering within the instrument makes it difficult to determine which lines are optically thick, and the resolution of the HETG makes it difficult to detect the putative higher ionization, faster wind component.

Also shown in Figure 6 is a simulated SXS spectrum. The observed continuum flux from GRO J1655–40 was approximately 1 Crab, which will give approximately 2000 c/s in the SXS. Turning off the central 5 pixels to optimize the number of high and medium resolution events that feed through the electronics will result in a H+M event rate of 60 c/s. In a 100 ks observation, the second ionization zone is easily detected with *ASTRO-H*, as can be seen from the blue wing on the Fe XXVI line that is not fit well by the one-zone model, and by an absorption line at 8 keV that is not addressed. Note also that the black lines are actually black, and incredibly well-separated.

3.4.2 Do Ultra-Fast Outflows (UFOs) Span the Mass Scale?

In deep spectra of Seyfert-1 AGN observed with *XMM-Newton* and *Suzaku*, a number of absorption lines may be detected that would signal winds with jet-like velocities (0.1–0.2 c in some cases (Tombesi et al., 2010a,b). These lines are of modest statistical significance after rigorous assessment via Monte Carlo techniques. These putative UFOs would surely have enormous impacts on their host environments, and confirming such outflows is therefore of high importance.

An extremely fast outflow has also been found in IGR J17091–3624, and at higher statistical significance than the AGN examples ($v = 0.03c$, King et al. 2012). Indeed, there is some evidence for two velocity systems, at 0.03 c and 0.05 c . This source is a “twin” of the near-Eddington microquasar GRS 1915+105, and if it also accretes near the Eddington limit, it would have another factor in common with AGN in which UFOs have been observed (the best case is likely PG 1211+143; Tombesi et al. 2010a). It is possible that high velocity outflows have previously eluded detection simply owing to a lack of sensitivity with increasing energy, both in CCD and gratings spectrometers. The energy resolution of the *ASTRO-H* SXS increases with energy, and will aid the detection of weak lines with strong velocity shifts.

Figure 7 shows a simulated 50 ksec SXS spectrum of IGR J17091–3624, next to the observed *Chandra* spectrum (King et al. 2012). The continuum measured in the HETG spectrum and XSTAR models used to analyze those data were used to simulate the SXS spectrum. The lower-velocity system is characterized by

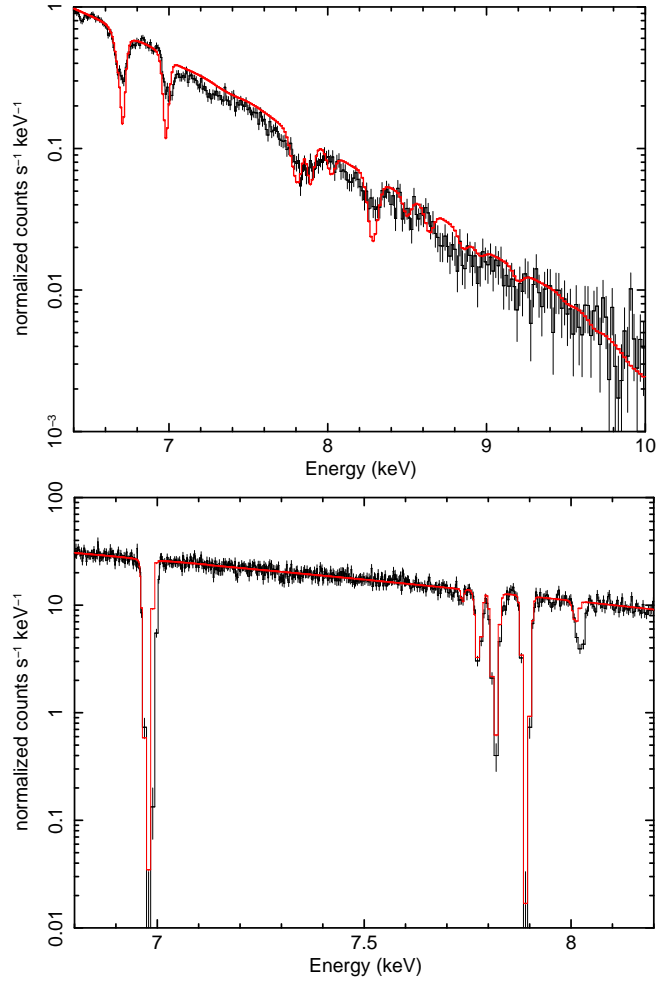


Figure 6: Top: The *Chandra*/HETG spectrum of GRO J1655–40 is shown here, fit with two XSTAR photoionization models: a dominant highly-ionization zone with a velocity of 400 km/s, plus a tentative even more highly ionized zone that is outflowing at an even higher velocity (1400 km/s). Bottom: A simulated 100 ks *ASTRO-H*/SXS spectrum is shown here, based on the model fit to the *Chandra* spectrum in the panel above. The model in red shows only the dominant zone in the panel above. The remaining blue flux in the Fe XXV He- α line at 6.700 keV and the strong blue flux in the line at 8 keV clearly show the need for the second zone. X-ray warm absorbers in Seyfert AGN are generally thought to be composed of at least two ionization zones; this simulation indicates that the *ASTRO-H*/SXS will be able to distinguish different zones within very ionized outflows, potentially building a stronger connection to X-ray warm absorbers in AGN.

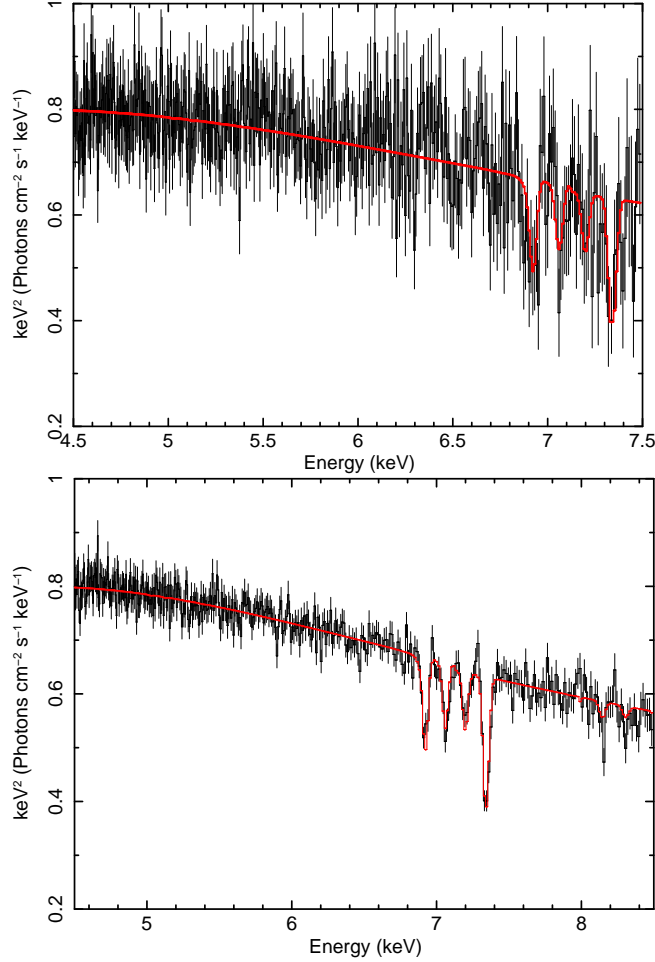


Figure 7: Top: A *Chandra*/HETG spectrum of IGR J170914–3624 is shown here, fit with two XSTAR photoionization zones. The outflow in this source is extreme; the components have velocities of $0.03c$ and $0.05c$ (King et al., 2012b). Bottom: This plot shows a simulated 50 ks spectrum, based on the model shown in the panel above. Whereas the components are difficult to detect with the *Chandra*/HETG, multiple fast outflow components can easily be detected, resolved, and separated at high resolution using the *ASTRO-H*/SXS.

$\log(\xi) = 3.3$ and $N_{\text{H}} = 4.7 \times 10^{21} \text{ cm}^{-2}$. The higher-velocity system is characterized by $\log(\xi) = 3.9$ and $N_{\text{H}} = 1.7 \times 10^{22} \text{ cm}^{-2}$. The flux measured with *Chandra* was approximately 0.1 Crab; this flux is likely to give about 200 c/s in the SXS. In this case, mitigations are not needed to cope with the count rate, and a H+M count rate of 60 c/s is anticipated. It is clear that both velocity systems are easily detected, and easily separated, in a modest observation.

4 Low-frequency variability

4.1 Links to accretion geometries

One of the best-known and most intriguing phenomena observed in both black-hole X-ray binaries and AGN is short-term X-ray variability. The fluctuations observed in many light curves are not periodic, nor random around some mean; rather, they seem to comprise numerous peaks (or shots) with different amplitudes and durations. Such variability may be a sort of $1/f$ noise, since its power spectrum exhibits a $f^{-\beta}$ decline at high frequencies (where f is the frequency and $1 < \beta < 2$ is a constant).

At low frequencies (below a few Hz), the power spectra are roughly flat. For this reason, the broad band variability observed in black holes is sometimes called low-frequency variability or low-frequency noise. Since

similar variability is commonly observed in other accretion systems, they are thought to be generic features of the accretion process, but there are still no widely accepted models despite intensive efforts having been done over many decades since its discovery.

The normalized power spectra are quite similar among different sources. As the total fractional variability increases (or decreases), the level of the flat part in the normalized power spectral densities (PSDs) also increases (decreases), while neither that of the power-law decline part nor its power-law slope changes significantly. That is, the break frequency separating the flat and power-law decline parts decreases (increases) accordingly. As a result, there is a linear correlation between the fractional variability and the break frequency (Belloni & Hasinger, 1990).

It is important to note that low frequencies mean long timescales. The timescale corresponding to a few Hz is a few tenths of a second, much longer than the dynamical timescale,

$$\tau_{\text{dyn}} \equiv \sqrt{\frac{r^3}{GM}} \simeq 4 \left(\frac{M}{10 M_{\odot}} \right) \left(\frac{r}{10 r_{\text{S}}} \right)^{3/2} \text{ ms} \quad (3)$$

(with M and r being the mass of a black hole and the distance from the black hole, respectively) or the thermal timescale ($= \tau_{\text{dyn}}/\alpha$ with $\alpha \sim 0.1$ being the viscosity parameter) of an accretion disk. By contrast, the viscous (accretion) timescale is much longer;

$$\tau_{\text{vis}} \equiv \frac{1}{\alpha} \left(\frac{r}{H} \right)^2 \sqrt{\frac{r^3}{GM}} \simeq 4 \left(\frac{\alpha}{0.1} \right)^{-1} \left(\frac{M}{10 M_{\odot}} \right) \left(\frac{T}{10^{10} \text{ K}} \right)^{-1} \left(\frac{r}{10 r_{\text{S}}} \right)^{1/2} \text{ s} \quad (4)$$

where H denotes the half-thickness of the flow, and T denotes its (ion) temperature. This means that X-ray variability is not a local phenomenon, but somehow reflects broader trends in the accretion rate. Indeed, the basic properties of the X-ray light curves can be reproduced by propagation of density fluctuations (e.g., Mineshige et al. 1994; Lyubarskii 1997).

Further, the character of the observed X-ray variability is closely related to the spectral state of the accretion disk. Rapid X-ray fluctuations are more pronounced during the hard (low) state and the “very high” state, although there exist small fluctuations during the soft state as well (Miyamoto et al., 1992). In contrast, variability is always observed in AGN. In both of the low/hard and very high states, radiation mainly originates in the hot accretion flow, rather than in the (relatively) cool, geometrically thin disk, which dominates in the high/soft state. Since magnetic activities are more enhanced in the hot accretion flow, X-ray variability could be caused by magnetic flares and the rapid release of magnetic energy, perhaps akin to solar flares.

4.2 Low-frequency QPOs and Lense-Thirring precession

Low frequency QPOs are commonly observed in the X-ray flux of both neutron star and black hole X-ray binaries. They are most clearly observed as strong, *incoherent* features in the power spectral density (PSD) which are Lorentzian in shape and so can be described by amplitude (i.e. fractional rms variability), centroid frequency (f_{QPO}) and width (Δf). These properties are observed to be correlated with the spectral properties of the source and with other noise components (see e.g. van der Klis 2006; Belloni 2010).

Different models exist for the evolution of accretion flows across an outburst, and numerous different models have been proposed to describe the “low/hard” state in particular and/or $L \ll L_{\text{Edd}}$ regimes generally (e.g. Esin et al. 1997; Beloborodov 1999; Blandford & Begelman 1999; Markoff et al. 2001; Taam et al. 2008; Meyer-Hofmeister et al. 2009). As the mass accretion rate through the disk falls, cooling will eventually fail and the inner disk will give rise to an inner hot accretion flow. The Eddington fraction at which this happens is uncertain, and it is possible that it may vary even for a given source, depending on whether the accretion rate is rising or falling. Positive evidence of an absent geometrical component is difficult to obtain, but some recent evidence suggests that disks may truncate at or below $0.001 L_{\text{Edd}}$ (Tomsick et al. 2009; Reis et al. 2009a, 2010)

The truncated disk model, in which the thin disk only extends down to some radius r_0 , can potentially explain the evolution of the SED (Esin et al., 1997; Done et al., 2007) and the correlated evolution of the power spectra

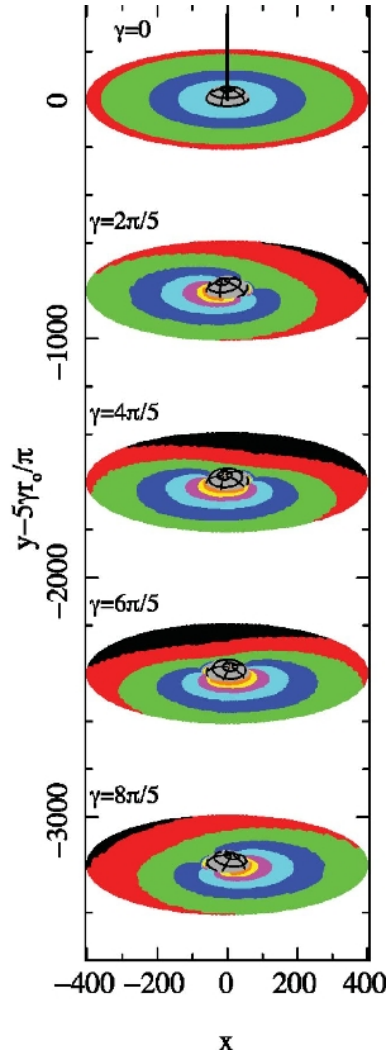


Figure 8: Lense-Thirring precession of a hot inner flow is predicted illuminate different azimuths of the disk as a function of QPO phase(Ingram & Done, 2011, 2012). This figure depicts a hot inner flow in gray with wire mesh, and the colors illustrate the intensity of illumination on the disk as the inner flow precesses.

(Ingram & Done, 2011, 2012). Interior to r_o is a large scale height, optically thin accretion flow which acts as the Comptonizing corona. As the source flux increases, the truncation radius moves inwards, thus increasing the flux of disk photons incident on the flow and softening the power-law emission while simultaneously decreasing all characteristic time scales associated with r_o . The evolution of both the energy spectra and power spectra imply that r_o moves from $\sim 60 - 6$ (in units of $R_g = GM/c^2$) during the rise to outburst and back out again during the fall back to quiescence.

This also gives a framework in which to incorporate the QPO and its properties via Lense–Thirring precession. This is a relativistic effect that occurs because a spinning compact object drags spacetime as it rotates. The orbit of a test particle that is outside the plane of black hole spin will therefore undergo precession because the starting point of the orbit rotates around the compact object. Stella & Vietri (1998) showed that the predicted frequency of a test mass at the truncation radius is broadly consistent with the observed QPO frequency and its evolution from $\sim 0.1 - 10$ Hz as r_o moves inwards and the source spectrum softens. However, the energy spectrum of the QPO is dominated by the Comptonized emission (Sobolewska & Życki, 2006; Rodriguez et al., 2004), requiring that the QPO mechanism predominantly modulates the hot flow rather than the disk (although the variability could be produced elsewhere before propagating into the flow; Wilkinson & Uttley 2009). Instead, a global precession of the entire hot flow modulates the Compton spectrum by the changing projected area of the flow as it precesses. This explains the QPO spectrum as well as its frequency, giving a physical model for the origin of the QPO which fits its known behaviour (Ingram et al., 2009).

One clear observational signature arising from this model, is that the flow preferentially illuminates different azimuths of the disk, giving rise to a periodically rocking of the reflected iron line between a red and blue shift (see Figure 9). There should be a clear pattern to the QPO, where the rising QPO amplitude means that the side of the disk coming towards us is illuminated giving a blue line, while the falling QPO phase illuminates the disk rotating away from us, giving a red line.

Indeed, earlier observational work was able to connect low–frequency QPOs to variations in Fe K lines, and the results were found to be consistent with Lense–Thirring precession. Miller & Homan (2005) found a link between Fe K line properties and the “phase” of very strong 1–2 Hz QPOs observed in GRS 1915+105 using *RXTE*. Unfortunately, the limited spectral resolution of *RXTE* prevented a detailed study of the line properties. However, based on that result, Schnittman et al. (2006) explored a model consisting of a precessing inner disk within a stable corona, and calculated the resulting line profile. This model differs from the model discussed above in some details, but the fact of competing theoretical frameworks and an encouraging observational result highlight the need to explore such phenomena using *ASTRO-H*.

This is not feasible to see with the SXS, as the upper limit of 35 c/s is too low to build-up enough statistics in a reasonable exposure time (see Figure 8). This count rate is a factor 50 below the *XMM-Newton* count rate seen in its high time resolution modes of a bright black hole binary. However, the HXI has no pileup issues. It also has an effective area (with 2 telescopes) that is comparable to the *RXTE/PCA* and larger than that of *XMM-Newton/EPIC*-pn camera above 6 keV. The energy resolution is comparable to the *RXTE/PCA*, especially when taking into account the fact that all fast time modes of the PCA were binned in energy resolution after the loss of the high gain antenna early in the mission. The HXI then has significant discovery space (along with *NuSTAR*) in terms of the spectra of fast time variability in black hole X-ray binaries.

Figure 9a shows a typical hard intermediate state spectrum such as seen from GX339–4 with a strong QPO as seen by *RXTE*. Simulating this through the HXI gives a count rate of 300 c/s for one telescope, so we double this to get the total count rate from both detectors. We construct a 100 ks HXI observation, as shown in figure 9b. Selecting data on rising phase and falling phase of the QPO then gives significantly different spectra. These are shown as a ratio to a power-law in figure 9c. This quasi-periodic shifting of the iron line peak energy with QPO phase is a prediction of the Lense–Thirring precession model for the low-frequency QPO that can be tested using the *ASTRO-H/HXI*.

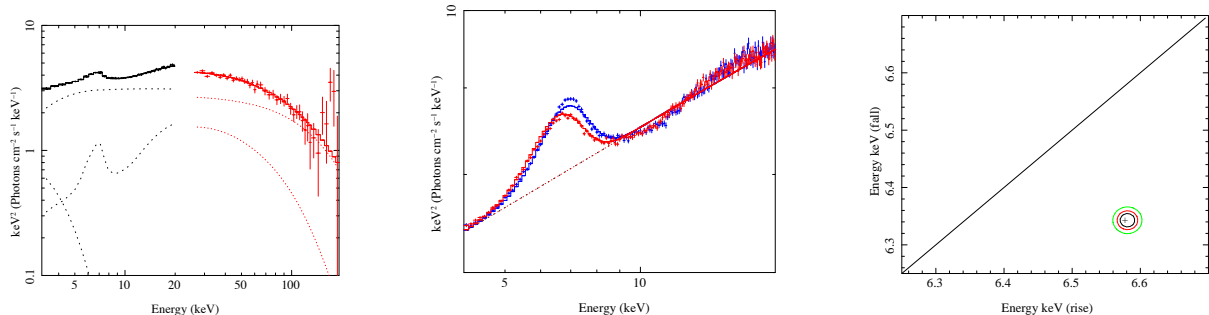


Figure 9: a) The *RXTE*/PCA and HEXTE data for a bright hard intermediate state of GX339-4 with strong QPO are shown here. b) A model simulated through the HXI and split into rising (blue) and falling (red) QPO phase is shown in this panel. c) This panel depicts the statistical confidence at which changes in line profile due to the QPO precession illuminating different azimuths can be detected (A. Ingram, private communication). The black, red, and green contours correspond to $\Delta\chi^2 = 2.3, 4.61, \text{ and } 9.21$, respectively.

4.3 Shot noise studies

Flux variability on \sim ms time scales (e.g., Miyamoto et al. 1992), seen in spectrally hard states, has been studied in many ways (e.g., Nowak et al. 1999; Poutanen 2001; Pottschmidt et al. 2003; Torii et al. 2011). However, the origin of such variability is still uncertain, presumably owing to the difficulty of realizing both high sensitivity and large effective area. A distinctive approach to understanding this variability is “shot analysis” (Negoro et al., 1994, 1995). The method is a time-domain stacking analysis to determine the universal properties behind non-periodic variability. Shot analysis makes it possible to combine timing analysis with spectral information in a straightforward manner. This technique was adopted for observations of Cyg X-1 obtained with *Ginga* (Turner et al., 1989), and was further explored with *RXTE* (Focke et al., 2005).

Shot analysis was recently applied to *Suzaku* data from Cygnus X-1 in an effort to better understand stochastic phenomena in a straightforward way (Yamada et al., 2013). In this work, the high energy limit of the shot analysis was extended up to ~ 200 keV, by utilizing data from both the HXD and XIS cameras. The interesting outcomes of this analysis include the following results:

- The shot feature is found at least up to ~ 200 keV, with high statistical significance.
- The shot profiles were found to be approximately symmetric, though the hardness changes progressively more asymmetrically toward higher energies of $E \gtrsim 100$ keV.
- The 10–200 keV spectrum at the peak shows a lower energy cut-off than the time-averaged spectrum.
- Within the framework of a single-zone Comptonization model for the cut-off, as a shot develops toward the peak, y and T_e decrease, while τ and the flux increase. Immediately after the shot peak, T_e and τ (and hence y) suddenly return to their time-averaged values. This fitting result and the spectrum at the peak, and that in 0.1 s before/after the peak are shown in figure 10.

The time constant of ~ 1 s far exceeds the local (dynamical or thermal) timescale of the innermost region, and should thus reflect the motion of particular gas elements. Manmoto et al. (1996) proposed an interesting explanation: that inward moving accreting blobs can cause an increase in X-ray flux, and this is reflected as sonic wave when it reaches the black hole (Kato et al., 2008). Rapid heating, such as might occur through magnetic

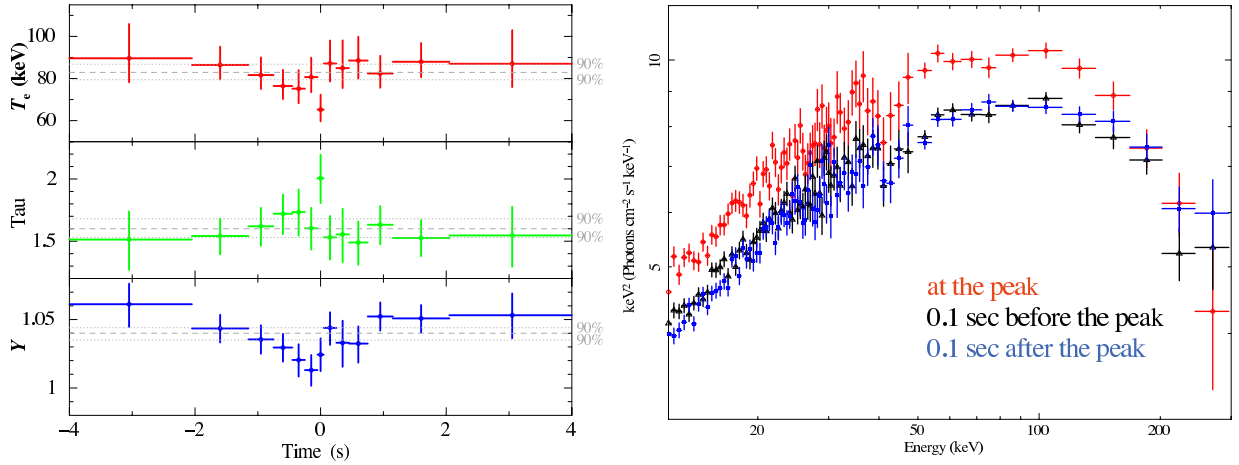


Figure 10: Left: The time evolution of parameters obtained from Comptonization modeling of *Suzaku* spectra of Cygnus X-1 are shown here. Fits were made to the 12–300 keV HXD spectra, in the 13 shot phases. From top to bottom, the electron temperature, the optical depth, and the Compton y parameter are presented. The 90% confidence range specified by the time-averaged spectrum is superposed by dotted and dashed lines. Right: The background-subtracted νF_ν HXD spectra, accumulated over different shot phases, are shown here (Yamada et al., 2013). The spectra were integrated from -0.25 to -0.05 seconds before the peak (black), from -0.05 to 0.05 seconds around the peak (red), and from 0.05 to 0.25 seconds after the peak (blue).

reconnection, can explain the short (~ 0.1 s) timescale of the shots, though the long (~ 1 s) timescale would be related to mass accretion time scale. Further observational studies are needed to completely understand the physics causing the rapid variability. For instance, shot profiles with distinct features, such as polarization (Laurent et al. 2011), γ -ray emission (Ling et al., 1987), or fine structures around Fe-K lines, all of which will be precisely measured by *ASTRO-H*, could provide a better understanding of the origin of the rapid flux variability.

5 Accretion flow evolution

5.1 Explorations of the low/hard state with *ASTRO-H*

The canonical “low/hard” state of black hole X-ray binaries actually encompass a large range in luminosity and accretion rate, with an upper bound of a $few \times 10^{-2} L_{Edd}$. Black holes transiting through the low/hard state from X-ray quiescence, or back into quiescence following an active period, can potentially be seen as the evolutionary link between LLAGNs (often observed at $\sim 10^{-6} L_{Edd}$, similar to the super-massive black hole in M81) and Seyfert AGN or even quasars accreting close to L_{Edd} .

It is generally agreed that the accretion flow properties and overall geometry of the inner regions surrounding black holes differ markedly between quiescent and quasar-like states. Sources that are inferred to accrete close to their Eddington limit reveal clear signatures of a standard optically-thick but geometrically-thin accretion disk extending close to the black hole. In such phases, a compact, hard X-ray emitting corona is also inferred through various means. In contrast, at very low fractions of the Eddington limit, a standard thin disk is replaced with a radiatively-inefficient accretion flow. So-called advection-dominated accretion flows (ADAFs, Narayan & Yi 1994; Esin et al. 1997) are the best known flavor of such models. Some studies have found that ADAFs are convectively unstable (Quataert & Gruzinov, 2000), and others have even found that the hot flow may not be bound to the black hole (Blandford & Begelman 1999). Whatever the details, it is clear that at some point during the low/hard state, the inner edge of the standard thin accretion disk must truncate. *ASTRO-H* will be able to incisively probe transient black hole binaries during the decline or rise of the low/hard state, down to luminosities $\sim 10^{-3} L_{Edd}$.

ASTRO-H will provide continuous, sensitive coverage in the 5–80 keV energy range via its HXI detector. It will enable the precise characterization of the disk reflection spectrum and a measure of the overall strength of

the Compton hump. Combined with simultaneous observations via the SGD – spanning energies up to 600 keV – *ASTRO-H* will be ideally suited to observe the expected spectral rollover in the 100 – 200 keV range due to thermal Comptonization in addition to disk reflection, and it will be able to do this fairly deep into the low/hard state. Simulations indicate that 100 ks observations of BHB at $\sim 10^{-2}L_{Edd}$ will provide reliable estimates of coronal temperatures, with errors no larger than 10% for corona temperatures as large as 200 keV.

The unprecedented resolution and sensitivity of the SXS in energies up to and beyond the Fe K region ($\sim 4\text{--}8$ keV), especially when combined with the HXI, will provide strong constraints on the inclination and ionization state of the accretion disk. These two parameters are derived partly based on the overall strength of the Compton hump at ~ 30 keV and the depth of the Fe K absorption edges in the 7.1–9.3 keV range. Simulations show that *ASTRO-H* will determine the ionization and inclination of systems like GX 339–4 at $\sim 10^{-2}L_{Edd}$ with 90% statistical errors of $\leq 1\%$ and $\leq 3\%$ respectively. For comparison, the equivalent precisions obtained without the soft X-ray coverage, are 13% and 22%, highlighting the immense importance of the broadband coverage provided by *ASTRO-H*.

The reprocessing of hard X-rays in the (relatively) cold accretion disk results in the production of several fluorescence and recombination lines; Fe K lines are merely the strongest in most circumstances. *ASTRO-H* will be sensitive to features from low- Z elements (Figure 11), and their detection will further constrain the ionization state of the accretion disk as the system evolves through the low/hard state. If the disk begins to recede at $L \sim 10^{-2}L_{Edd}$, *ASTRO-H* – due to its broadband coverage and highly sensitive soft X-ray detector – will be in a position to map this evolution with 90% statistical errors of less than 10% for an inner accretion disk radius of $10 R_g$ at $L \sim 1 \times 10^{-2}L_{Edd}$ and 35% for a disk at $100 R_g$ at $1.4 \times 10^{-3}L_{Edd}$.

5.2 Tests of the hard X-ray corona with *ASTRO-H*

A power-law spectral component is particularly prominent in the X-ray spectra of black hole X-ray binaries in the “low/hard” and “very high” states. Similar components are observed in the X-ray spectra of Seyfert AGN. Inverse Comptonization of soft photons from an (optically thick) accretion disk by electrons in an (optically thin) corona is one plausible means of generating power-law X-ray emission. The corona is generally characterized with electron temperatures of 10^9 K and the Compton y parameter of 1, according to hard X-ray observations of black hole X-ray binaries and a limited number of Seyferts.

Very recently, a high energy cut-off was detected in the spectra of several NLS1s (a class of radio quiet AGNs with low black hole masses and high accretion rate), and some of the sources show electron temperatures lower than 60 keV (e.g. Malizia et al., 2009). Changes in the electron temperature were also recently observed in the Seyfert 1.9 NGC 4151: $kT_e = 50\text{--}70$ keV was recorded in a bright state, while $kT_e = 180\text{--}230$ keV was measured in a dim state (Lubiński et al., 2010). These results are consistent with the thermal Comptonization model, considering the Compton cooling is more efficient for a larger accretion rate.

Extensive studies have been made to account for the X-ray power-law component and its high energy cut-off in terms of a coupled disk–plus–corona system (e.g. Haardt & Maraschi 1991; Liu et al. 2003; Kawabata & Mineshige 2010; Meyer-Hofmeister et al. 2012). A significant fraction of energy can be dissipated in the corona, even when mass is accreted primarily through the disk. Ions in corona are typically assumed to be fully ionized in these studies. According to Liu et al. (2002), the ion temperature is as high as 10^{11} K, two orders of magnitude higher than the electron temperature at the vicinity of a central black hole. The ion temperature is 10^{12} K in ADAF models (e.g. Narayan & Yi 1994). However, the low electron temperatures derived from model–dependent fits to the spectra of some sources are not in the range of these theoretical models. Furthermore, considering the fact that evaporation and condensation of materials between corona and disk must happen, there could be ions with temperatures between the disk temperatures ($10^5 - 10^7$ K) and the corona temperatures ($10^9 - 10^{11}$ K).

The combined capabilities of the *ASTRO-H/SXS* and HXI may be able to detect the presence of partially-ionized (or even neutral) ions within the corona. This may be of particular importance in low–temperature coronae with high optical depth, like those noted in the above discussion. Rather than a smooth continuum, cooler components within the corona may have the effect of causing atomic absorption features, and a partic-

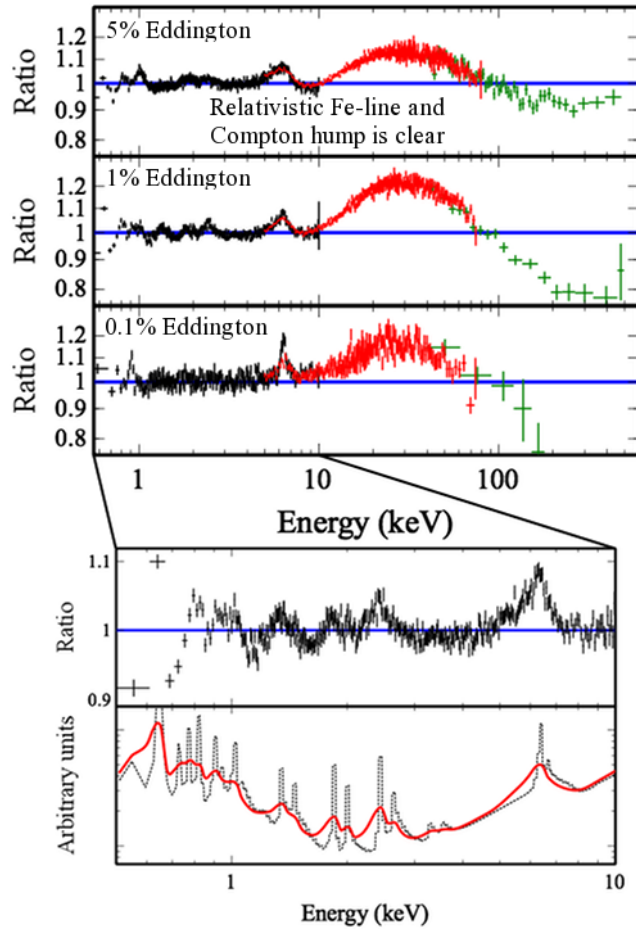


Figure 11: Simulated data-to-model ratio of GX 339–4 at $L/L_{Edd} = 5, 1$ and 0.1% . The inner accretion disk is assumed to extend to the ISCO at $2.32 R_g$ at $L/L_{Edd} = 0.05$ and increase to $10 R_g$ and $100 R_g$ as the luminosity decreases. In all cases, the simulated spectra were fit with an absorbed power-law together with a thermal disk component with the iron line and Compton hump energies excluded from the fit. These figures show that *ASTRO-H* will detect the clear signatures of reprocessed emission from which the radius of the accretion disk can be measured. The close up shows the data-to-model ratio for the system at 1% Eddington (top) with the plot below showing the expected signatures from reflection before (black) and after (red) the effects of strong gravity.

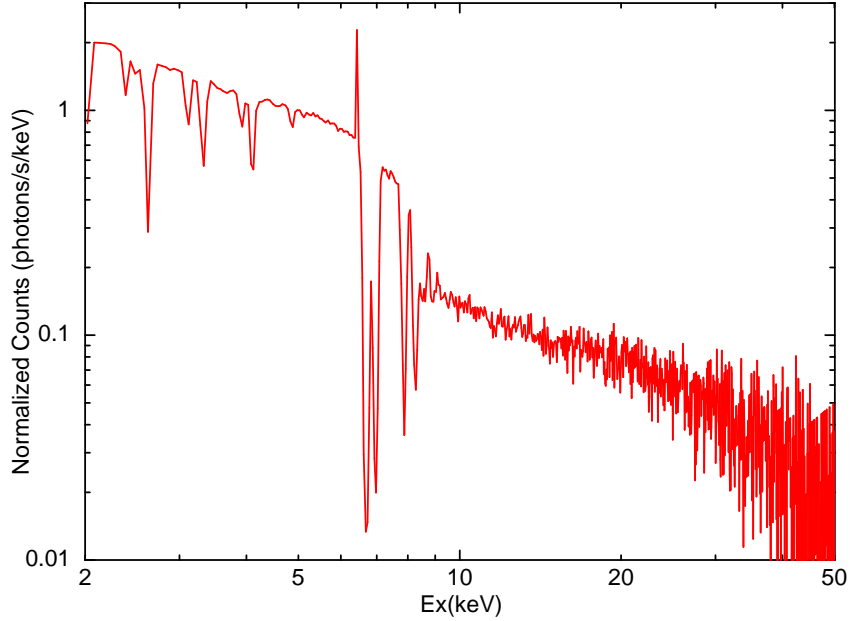


Figure 12: Preliminary simulation of an emergent (model) spectrum from a partially ionized corona. The corona is assumed to be a sphere of Compton optical depth $\tau = 5$ and $kT_e = kT_i = 10$ keV. Soft photons are injected at its center. These parameters represent a rather extreme case for demonstration, though a step like feature is found at iron K band.

ularly pronounced step in the region of the Fe K edges (Hayashida et al., 2007). Figure 12 shows a simulated *ASTRO-H* spectrum based on the mixed corona model of Hayashida et al. (2007).

5.3 X-ray Continuum Emission

Establishing a complete picture of the geometry and emission mechanisms in the central accretion flow onto black holes remains an important observational goal. The primary X-ray continuum in Seyfert-I AGN, perhaps partially arising through Comptonization in coronae near the black hole, has long been approximated by a single power-law. Novel techniques - such as the construction of difference spectra - can reveal the nature of the primary continuum; deep observations suggest that it obeys a power-law form to within 10% in the 3–10 keV band (Vaughan & Fabian, 2004). X-ray spectroscopy of Seyferts has therefore focused on deviations from a power-law continuum, including complex absorbers, reflection, and fluorescence lines.

However, broad-band *Suzaku* studies of several Seyfert-1s, utilizing a novel variability-assisted spectroscopy method called the C3PO (Count-Count Correlation with Positive Offset) method, has suggested that the continuum may consist of multiple primary emission components (Noda et al., 2011a,b). This means that the Compton coronae constituting the central engines of AGN may consist of multiple zones, as was suggested for some black hole X-ray binaries (e.g., Makishima et al. 2008), in contrast to the conventional belief of a single-zone corona.

Owing to the higher flux observed from Galactic stellar-mass black holes, such techniques may be even more profitably employed to understand continuum emission in these sources. In this regard, the broad-band spectral coverage and time resolution of the HXI and SGD will be especially important (see Figure 13). Even snapshot broadband spectra of bright stellar-mass black holes with *ASTRO-H* can potentially reveal any disagreement with simple, single-zone coronae.

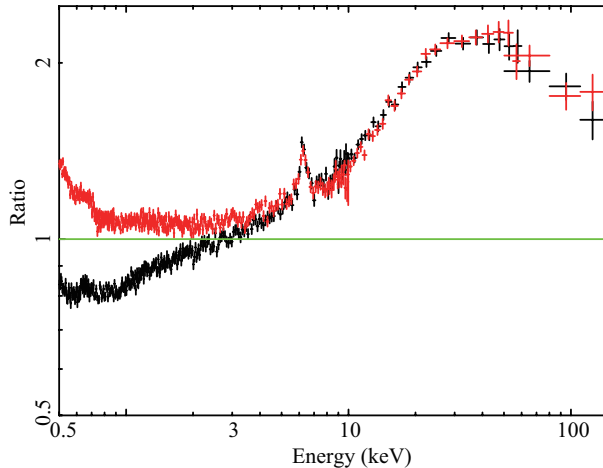


Figure 13: Simulated *ASTRO-H* spectra of the type I Seyfert Mrk 509 are shown here, in ratio to a $\Gamma = 2$ power-law continuum. The spectra were generated assuming the two best-fit models for the *Suzaku* spectra of Mrk 509 obtained on 2006 April 25 and November 15 (Noda et al. 2011b). An exposure of 100 ksec is assumed for each. Spectra of this quality may help to better understand the nature of the X-ray continuum.

6 Super-Eddington Accretion

6.1 Current Ideas

Current observational knowledge of black hole accretion is largely restricted to sub-Eddington regimes, in which the (disk) luminosity is below the Eddington luminosity, $L_E \sim 1.3 \times 10^{39} (M/10 M_\odot) \text{ erg s}^{-1}$. When the luminosity approaches the Eddington limit, the radiation field exerts a strong pressure force against gas that is drawn inward by gravitation, resulting in a powerful outflow. The large mass outflow rate affects the accretion flow structure, as well as the local environment. Thus, super-Eddington (or supercritical) accretion is inhibited in a spherical geometry.

Supercritical accretion may be possible through an accretion disk, however, since the radiation pressure force and gravitational force are not direct opposition at all points. Even in a supercritical disk accretion geometry, radiation and matter are strongly coupled. This again causes a radiation-pressure driven outflow near the flow surface, and photon trapping deep inside the accretion flow. The critical radius separating the inner, nearly isotropic outflow region and the outer accretion region is called the spherization radius, which increases as the accretion rate (\dot{M}) increases (Shakura & Sunyaev, 1973). There is another critical radius, the photon trapping radius. Within this radius, photons are "trapped" within the flow, and, hence, radiative efficiency is somewhat reduced (Abramowicz et al. 1988, see also Chap. 10 of Kato et al. 2008). Numerically, the photon trapping radius is roughly equal to the spherization radius; that is, these two effects work simultaneously. The photon trapping occurs also in neutron star accretion but only temporarily, since all the photons produced within the accretion flow onto stars with solid a surface should be eventually emitted.

To understand strong and complex matter-radiation interactions, global radiation- hydrodynamic and/or radiation- MHD simulations have recently been undertaken, and have predicted a number of features that may be characteristic of a supercritical flow, such as mild beaming (anisotropic radiation fields), the emergence of relativistic, collimated jets, and loosely-collimated outflows with moderately high velocity ($\sim 0.1c$) and internal circulation (Ohsuga et al., 2005, 2009). As a result of the mild beaming, the maximum apparent luminosities can exceed $10L_E$ for face-on observers. The relativistic jets are accelerated by radiation pressure, and they are collimated by magnetic force and/or pressure from a surrounding, geometrically thick disk (Takeuchi et al., 2010). The outflow is of particular importance, since it carries a large mass flux, $\dot{M}_{\text{outflow}} \sim 10L_E/c^2$, momentum, $\sim L_E/c$, and kinetic energy, $\sim 0.1L_E/c^2$. The outflow tends to have highly clumpy structure (Takeuchi et al., 2013), which may cause variability.

These predicted features of super-Eddington flows are best studied in X-rays. The most important observational features that can be pursued with *ASTRO-H* are (1) persistent relativistic jets, (2) line absorption features

by high-velocity outflow materials, and (3) significant Comptonization by hot outflow gas in continuum spectra.

6.2 SS 433 with *ASTRO-H*

SS 433 is a 13.1-d binary with a pair of precessing jets with a (nearly constant) speed of $0.26c$. It is the only source among all the classes of astrophysical jets that shows unambiguous signature of baryonic matter accelerated to a significant fraction of the speed of light. The jet is composed of normal hot plasma that gradually cools as it travels, producing a multi-temperature thermal emission spectrum. The part of the jet near the base, with a temperature of $kT > 10$ keV, emits strong X-ray lines from heavy elements. Further out in the jet, at distances $> 10^{12}$ cm, the plasma emits $H\alpha$ lines that vary in wavelength with the ~ 163 -d precession period. The geometry of the jet is well described by the “kinetic model”; the inclination of the precession axis is $i = 79^\circ$ and the precession cone angle is $\theta = 20^\circ$ (see Figure 14).

SS 433 is the only jet source that has yielded such detailed information on the geometry and the thermal structure of the jet, and therefore it represents a rare window on the physical processes that drive jet production. It may also hold clues to supercritical accretion and ULXs: the size, density and thermal structure of the X-ray emitting jet was spatially resolved by the eclipse mapping technique using *ASCA* data (Kotani et al., 1996), and one of the most important conclusions of the analysis is the kinetic power of the jet is $L_{kin} \geq 10^{40}$ erg s $^{-1}$, far greater the apparent X-ray luminosity ($L_{rad} \sim 10^{36}$ erg s $^{-1}$).

Observations of SS 433 with *ASTRO-H* will bear in the following problems:

- It is not yet clear how the jet of SS 433 is collimated into a narrow cone angle (< 0.1 rad), and then accelerated to a constant speed of $0.26c$. Namiki et al. (2003) found the Fe K lines are broader than lines from lighter elements in the *Chandra* HETG spectrum, hinting that the jet is gradually collimated over a length of $> 10^{10}$ cm as it cools. Using the eclipse mapping on the *ASTRO-H* spectrum, it should be possible to measure the radial velocity and width of emission lines as a function of the position for each of the approaching and receding jets. The same data can greatly improve upon estimates of the plasma condition, the jet power, and the geometry of the accretion disk over the previous studies.
- The striking disparity between the kinetic power of the jet $L_{kin} \geq 10^{40}$ erg s $^{-1}$ and the apparent X-ray luminosity ($L_{rad} \sim 10^{36}$ erg s $^{-1}$) may indicate that there are strong radiation beams co-aligned with the jets that never point to us. The ionized absorption edges and fluorescence lines found in the *Suzaku* spectra of SS 433 (Kubota et al., 2010b) suggest such beamed radiation may be present in the system. If the putative beamed emission from this source is confirmed with *ASTRO-H*, it may have important implications for ULXs in nearby galaxies.
- The nature of the compact object in SS 433 is not yet known. The mass of the compact object (M_x) has been estimated based on the measured Keplerian velocities of the compact object and the donor star. One current estimate, $1.9 < M_x/M_\odot < 4.9$ (Kubota et al., 2010a), favors a small-mass black hole, but a heavy neutron star cannot be ruled out. Measurements of the radial velocity amplitude of the stationary 6.4 keV Fe line, which may originate in the accretion disk, can improve the accuracy of mass constraints.
- X-ray lobes (Yamauchi et al., 1994) are located at $\sim 40''$ on the east and west sides of SS 433. They are aligned with the axis of the precessing jet as determined in radio imaging. It is natural to assume that they are powered by the jet, and represent the dissipation of the bulk kinetic energy of the jet in the shock, *i.e.* either the termination shock of the jet against the ISM or the internal shock of the colliding loops of the jet spiral. The absence of emission lines in *ASCA* spectra of the lobes suggests that the emission is non-thermal, but this needs to be confirmed with the SXS and HXI. The HXI image and spectra will clarify the emission process, and enable calorimetry of the jet. The detection of any thermal component in the shock would provide additional information on the dissipation of the jet.

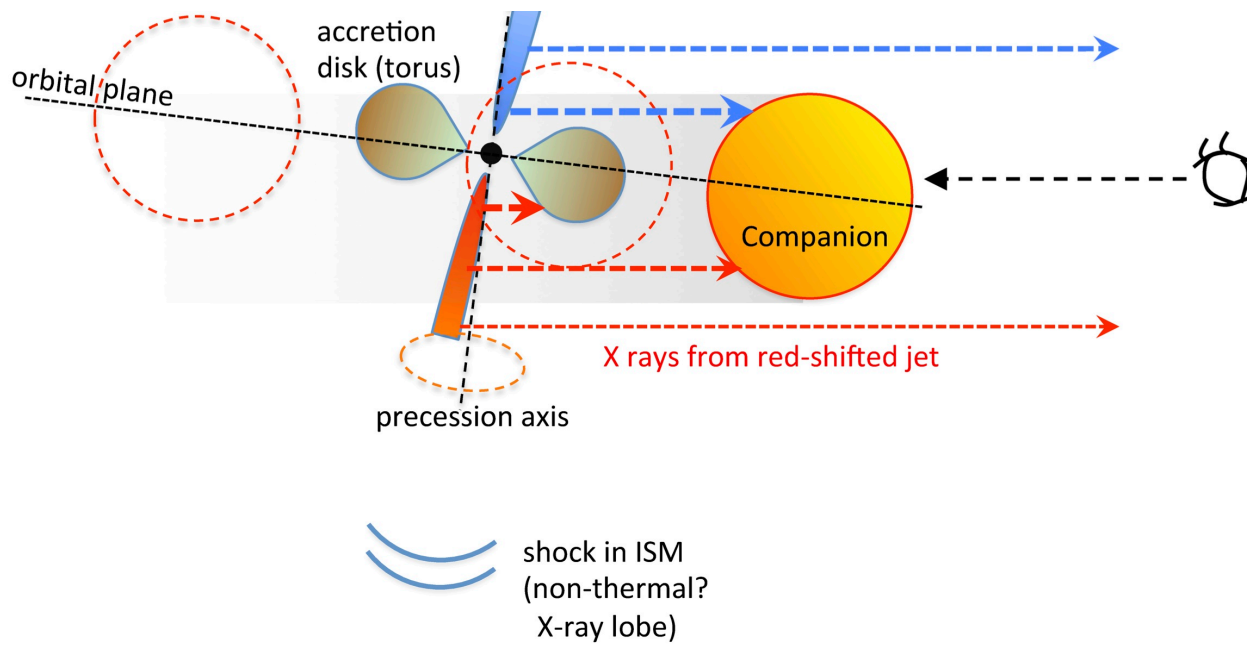


Figure 14: The schematic view of the SS 433 system.

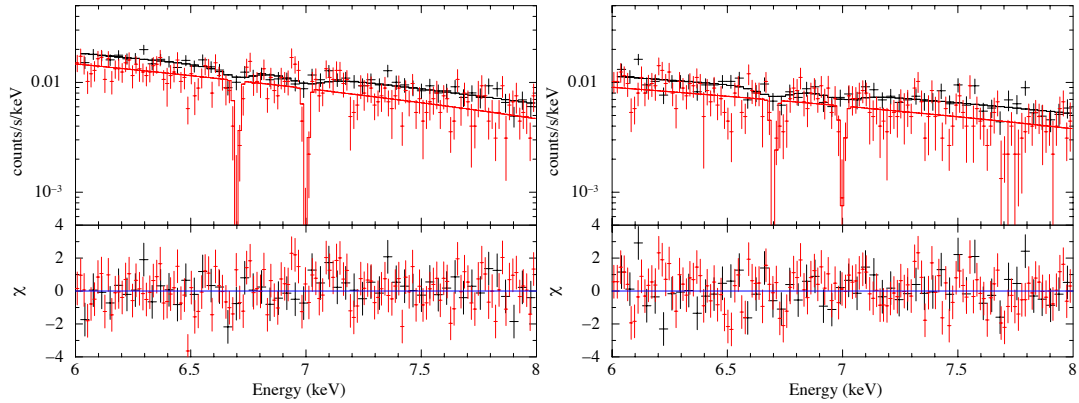


Figure 15: Simulated SXS (red) and HXI (black) spectra are shown above, based on the high (left) and low (right) states observed in the ULX IC 342 X-1 by Yoshida et al. (2013). The source luminosity was 1×10^{40} erg s^{-1} , and 5×10^{39} erg s^{-1} in the high and low state, respectively. In 150 ks of exposure, He-like and H-like Fe absorption lines with equivalent widths above 30 eV can be detected at more than 99.9% confidence, and the velocity shifts of the lines can be well determined to within 250 km/s. In the figures above, equivalent widths of 40 eV were assumed, and the spectra are binned for visual clarity.

6.3 Models for ULXs

Ultraluminous X-ray sources (ULXs) are off-nuclear X-ray point-like sources with large luminosities exceeding the Eddington luminosity of stellar mass black holes (see, e.g., Miller & Colbert 2004; Schartel 2011; Walton et al. 2011). Despite extensive studies over three decades, the nature of the central engine in ULXs remains an open question. However, it is likely that ULXs represent a new sort of accretion flow: subcritical accretion onto intermediate-mass black holes (IMBHs; $M \geq 100M_{\odot}$; e.g. Makishima et al. 2000; Godet et al. 2009; Webb et al. 2010; Sutton et al. 2012), or supercritical accretion onto stellar-mass black holes (e.g. King et al. 2001; Watarai et al. 2001). Of course, it is possible that the class encompasses both source types.

Each hypothesis has pros and cons. Some ULXs show blackbody-like spectra whose temperatures are $kT \sim 0.2$ keV, indicating large innermost radii, and suggesting a black hole mass within the IMBH range (e.g. Miller, Fabian, & Miller 2004a), while some others show rather high temperatures, > 1 keV, potentially supporting the supercritical scenario (e.g. Vierdayanti et al. 2006b). The discovery of very low frequency QPOs (Strohmayer & Mushotzky 2009) also supports the IMBH hypothesis. From the viewpoint of the star formation theory, however, it is difficult to form an IMBH (e.g. Madhusudhan et al. 2006). Optical nebulae surround some ULXs and have been used as bolometers; this technique suggests large luminosities and also favors IMBHs (see, e.g., Pakull & Mirioni 2002; Kaaret et al. 2004). Sustained fuelling of the accretion flow is difficult in both scenarios.

In any case, these are new possibilities and their unique properties must be explored both observationally and theoretically. Studies with *ASTRO-H* are expected to open new windows. If the supercritical accretion scenario is correct, we expect absorption features in the SXS spectra produced by strong outflow associated with supercritical flow. Recent work has placed very strong limits on the equivalent width of emission and absorption lines in Ho IX X-1 and NGC 1313 X-1 (Walton et al., 2012). The upper limit obtained for Ho IX X-1, just 30 eV, is within the range of absorption line strengths detected in Galactic black hole X-ray binaries, and an order of magnitude below the expected line strength of the mass outflow rate scales with the inflow rate. A deep, extremely sensitive SXS spectrum may finally be able to detect absorption lines consistent with a super-Eddington wind.

An example of the ability of *ASTRO-H* to decisively detect or reject the outflows expected from super-Eddington accretion is shown in Figure 15. Two states of the well-known ULX IC 342 X-1 are simulated, based on the continua and flux levels reported by Yoshida et al. (2013). Narrow lines from He-like and H-like Fe can be detected at greater than the 99.9% confidence level in a 150 ks exposure, assuming equivalent widths of 30 eV (comparable to current limits).

It is also essential to obtain *broad* band spectra of ULXs (up to a few hundreds of keV) with SXI and HXI for the first time to establish similarities and differences between ULXs, Galactic black hole binaries (BHBs),

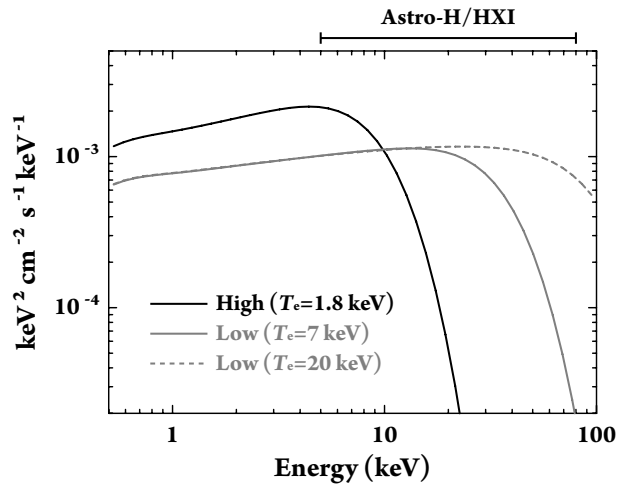


Figure 16: Expected spectral energy distributions (based on a Comptonization model for ULXs; see Yoshida et al. (2013)) with parameters of IC 342 X-1 during its power-law (PL) state: $(kT_e, \tau) = (1.8 \text{ keV}, 8.5)$ by the black solid line, $(7 \text{ keV}, 3.6)$ by the gray solid line, and $(20 \text{ keV}, 1.8)$ by the gray dashed line, respectively. The seed photon temperature of both states is assumed to be 0.1 keV. The energy range of the *ASTRO-H* is shown at the top-right corner. Adopted from Yoshida et al. (2013).

and AGNs. Like Galactic BHBs, ULXs exhibit spectral state transitions, however, the relationship between the spectral states and luminosities, and with timing properties are poorly investigated.

The spectra of some ULXs can be interpreted as the result of thermal Comptonization by relatively low-temperature electrons ($kT_e \approx 5 \text{ keV}$), much lower than those found in other black hole systems (with $\sim 100 \text{ keV}$). Gladstone et al. (2009) defined a state encompassing such spectra, the “ultra-luminous” state (see also Vierdayanti et al. 2010). This spectral decomposition is in agreement with some simulations (Kawashima et al., 2012), and provides support for the supercritical scenario. If this scenario is correct, we should see a spectral turnover in the hard X-ray range.

The same is true for another state of ULXs, the power-law spectral state. Physical understanding of the power-law spectra of ULXs is a potential key to a deeper understanding of the nature of ULXs, since the supercritical scenario predicts a spectral turnover in the hard X-ray band (Yoshida et al. 2013; see figure 16). If the power-law spectral component extends up to $\sim 100 \text{ keV}$, ULXs are more likely to be normal mode of accretion; that is, the IMBH hypothesis is supported. Clearly, the existence or absence of a break in the power-law tail, will give us important information regarding the physical situations of ULXs.

References

- Abramowicz M. A., Czerny B., Lasota J. P., Szuszkiewicz E., 1988, *ApJ*, 332, 646
- Allen S. W., Dunn R. J. H., Fabian A. C., Taylor G. B., Reynolds C. S., 2006, *MNRAS*, 372, 21
- Atoyan A. M., Aharonian F. A., 1999, *MNRAS*, 302, 253
- Balbus S. A., Hawley J. F., 2002, *ApJ*, 573, 749
- Bardeen J. M., Press W. H., Teukolsky S. A., 1972, *ApJ*, 178, 347
- Barr P., White N. E., Page C. G., 1985, *MNRAS*, 216, 65P
- Beckwith K., Done C., 2004, *MNRAS*, 352, 353
- Begelman M. C., McKee C. F., Shields G. A., 1983, *ApJ*, 271, 70
- Belloni T. M., 2010, in T. Belloni ed., *Lec. Notes in Physics*, Berlin Springer Verlag Vol. 794, Lecture Notes in Physics, Berlin Springer Verlag. p. 53, arXiv:0909.2474, doi:10.1007/978-3-540-76937-8_3
- Belloni T., Hasinger G., 1990, *A&A*, 227, L33
- Beloborodov A. M., 1999, *ApJ*, 510, L123
- Berti E., Volonteri M., 2008, *ApJ*, 684, 822
- Bhattacharyya S., Strohmayer T. E., 2007, *ApJ*, 664, L103
- Blaes O. M., Davis S. W., Hirose S., Krolik J. H., Stone J. M., 2006, *ApJ*, 645, 1402
- Blandford R. D., Begelman M. C., 1999, *MNRAS*, 303, L1
- Blandford R. D., Payne D. G., 1982, *MNRAS*, 199, 883
- Blandford R. D., Znajek R. L., 1977, *MNRAS*, 179, 433
- Blum J. L., Miller J. M., Cackett E., Yamaoka K., Takahashi H., Raymond J., Reynolds C. S., Fabian A. C., 2010, *ApJ*, 713, 1244

- Boirin L., Parmar A. N., 2003, *A&A*, 407, 1079
- Boirin L., Parmar A. N., Barret D., Paltani S., Grindlay J. E., 2004, *A&A*, 418, 1061
- Cackett E. M., et al., 2008, *ApJ*, 674, 415
- Cackett E. M., et al., 2010, *ApJ*, 720, 205
- Cackett E. M., Fabian A. C., Zoghbi A., Kara E., Reynolds C., Uttley P., 2012, *ArXiv e-prints*,
- Calvet N., Hartmann L., Kenyon S. J., 1993, *ApJ*, 402, 623
- Chartas G., Kochanek C. S., Dai X., Poindexter S., Garmire G., 2009, *ApJ*, 693, 174
- Chartas G., Kochanek C. S., Dai X., Moore D., Mosquera A. M., Blackburne J. A., 2012, *ArXiv e-prints*,
- Church M. J., Reed D., Dotani T., Bałucińska-Church M., Smale A. P., 2005, *MNRAS*, 359, 1336
- Coppi P. S., 1999, in J. Poutanen & R. Svensson ed., *Astronomical Society of the Pacific Conference Series Vol. 161, High Energy Processes in Accreting Black Holes*. pp 375–+, [arXiv:astro-ph/9903158](https://arxiv.org/abs/astro-ph/9903158)
- Crenshaw D. M., Kraemer S. B., 2012, *ApJ*, 753, 75
- Doeleman S. S., et al., 2008, *Nat*, 455, 78
- Doeleman S. S., et al., 2012, *Science*, 338, 355
- Done C., Gierliński M., Kubota A., 2007, *A&AR*, 15, 1
- Dovčiak M., Muleri F., Goosmann R. W., Karas V., Matt G., 2008, *MNRAS*, 391, 32
- Esin A. A., McClintock J. E., Narayan R., 1997, *ApJ*, 489, 865
- Fabian A. C., Sanders J. S., Taylor G. B., Allen S. W., Crawford C. S., Johnstone R. M., Iwasawa K., 2006, *MNRAS*, 366, 417
- Fabian A. C., et al., 2009, *Nat*, 459, 540
- Fabian A. C., et al., 2012, *ArXiv e-prints*,
- Farrell S. A., Webb N. A., Barret D., Godet O., Rodrigues J. M., 2009, *Nat*, 460, 73
- Fender R. P., 2001, *MNRAS*, 322, 31
- Fender R. P., Belloni T. M., Gallo E., 2004, *MNRAS*, 355, 1105
- Fender R. P., Gallo E., Russell D., 2010, *MNRAS*, 406, 1425
- Ferland G. J., Korista K. T., Verner D. A., Ferguson J. W., Kingdon J. B., Verner E. M., 1998, *PASP*, 110, 761
- Focke W. B., Wai L. L., Swank J. H., 2005, *ApJ*, 633, 1085
- Gammie C. F., Shapiro S. L., McKinney J. C., 2004, *ApJ*, 602, 312
- Georganopoulos M., Aharonian F. A., Kirk J. G., 2002, *A&A*, 388, L25
- George I. M., Fabian A. C., 1991, *MNRAS*, 249, 352
- Gierliński M., Middleton M., Ward M., Done C., 2008, *Nat*, 455, 369
- Gladstone J. C., Roberts T. P., Done C., 2009, *MNRAS*, 397, 1836
- Godet O., Barret D., Webb N. A., Farrell S. A., Gehrels N., 2009, *ApJ*, 705, L109
- Haardt F., Maraschi L., 1991, *ApJ*, 380, L51
- Hawley J. F., Krolik J. H., 2001, *ApJ*, 548, 348
- Hayashida K., et al., 2007, *Progress of Theoretical Physics Supplement*, 169, 269
- Hiemstra B., Méndez M., Done C., Díaz Trigo M., Altamirano D., Casella P., 2011, *MNRAS*, 411, 137
- Hjellming R. M., Rupen M. P., 1995, *Nat*, 375, 464
- Ingram A., Done C., 2011, *MNRAS*, 415, 2323
- Ingram A., Done C., 2012, *MNRAS*, 419, 2369
- Ingram A., Done C., Fragile P. C., 2009, *MNRAS*, 397, L101
- Kaaret P., Ward M. J., Zezas A., 2004, *MNRAS*, 351, L83
- Kallman T. R., McCray R., 1982, *ApJS*, 50, 263
- Kallman T. R., Angelini L., Boroson B., Cottam J., 2003, *ApJ*, 583, 861
- Kallman T. R., Bautista M. A., Goriely S., Mendoza C., Miller J. M., Palmeri P., Quinet P., Raymond J., 2009, *ApJ*, 701, 865
- Kato S., Fukue J., Mineshige S., 2008, *Black-Hole Accretion Disks — Towards a New Paradigm —*
- Kawabata R., Mineshige S., 2010, *PASJ*, 62, 621
- Kawashima T., Ohsuga K., Mineshige S., Yoshida T., Heinzeller D., Matsumoto R., 2012, *ApJ*, 752, 18
- King A. R., Davies M. B., Ward M. J., Fabbiano G., Elvis M., 2001, *ApJ*, 552, L109
- King A. L., et al., 2011, *ApJ*, 729, 19
- King A. L., Miller J. M., Raymond J., 2012a, *ApJ*, 746, 2
- King A. L., et al., 2012b, *ApJ*, 746, L20
- King A. L., et al., 2013, *ApJ*, 762, 103
- Kotani T., Kawai N., Matsuoka M., Brinkmann W., 1996, *PASJ*, 48, 619
- Kotani T., Ebisawa K., Dotani T., Inoue H., Nagase F., Tanaka Y., Ueda Y., 2000, *ApJ*, 539, 413
- Kraemer S. B., et al., 2005, *ApJ*, 633, 693
- Kubota A., et al., 2007, *PASJ*, 59, 185
- Kubota K., et al., 2010a, *PASJ*, 62, 323

- Kubota K., Ueda Y., Fabrika S., Medvedev A., Barsukova E. A., Sholukhova O., Goranskij V. P., 2010b, *ApJ*, 709, 1374
- Laurent P., Rodriguez J., Wilms J., Cadolle Bel M., Pottschmidt K., Grinberg V., 2011, *Science*, 332, 438
- Lee J. C., Reynolds C. S., Remillard R., Schulz N. S., Blackman E. G., Fabian A. C., 2002, *ApJ*, 567, 1102
- Levinson A., Blandford R., 1996, *ApJ*, 456, L29
- Ling J. C., Mahoney W. A., Wheaton W. A., Jacobson A. S., 1987, *ApJ*, 321, L117
- Liu B. F., Mineshige S., Meyer F., Meyer-Hofmeister E., Kawaguchi T., 2002, *ApJ*, 575, 117
- Liu B. F., Mineshige S., Ohsuga K., 2003, *ApJ*, 587, 571
- Lubiński P., Zdziarski A. A., Walter R., Paltani S., Beckmann V., Soldi S., Ferrigno C., Courvoisier T. J.-L., 2010, *MNRAS*, 408, 1851
- Luketic S., Proga D., Kallman T. R., Raymond J. C., Miller J. M., 2010, *ApJ*, 719, 515
- Lyubarskii Y. E., 1997, *MNRAS*, 292, 679
- Maccarone T. J., 2002, *MNRAS*, 336, 1371
- Machida M., Nakamura K., Matsumoto R., 2004, *PASJ*, 56, 671
- Madhusudhan N., Justham S., Nelson L., Paxton B., Pfahl E., Podsiadlowski P., Rappaport S., 2006, *ApJ*, 640, 918
- Magdziarz P., Zdziarski A. A., 1995, *MNRAS*, 273, 837
- Mahadevan R., Quataert E., 1997, *ApJ*, 490, 605
- Makishima K., et al., 2000, *ApJ*, 535, 632
- Makishima K., et al., 2008, *PASJ*, 60, 585
- Malizia A., Stephen J. B., Bassani L., Bird A. J., Panessa F., Ubertini P., 2009, *MNRAS*, 399, 944
- Manmoto T., Takeuchi M., Mineshige S., Matsumoto R., Negoro H., 1996, *ApJ*, 464, L135
- Markoff S., Falcke H., Fender R., 2001, *A&A*, 372, L25
- Matsumoto H., Tsuru T. G., Koyama K., Awaki H., Canizares C. R., Kawai N., Matsushita S., Kawabe R., 2001, *ApJ*, 547, L25
- Mauche C. W., Raymond J. C., 2000, *ApJ*, 541, 924
- McClintock J. E., Shafee R., Narayan R., Remillard R. A., Davis S. W., Li L., 2006, *ApJ*, 652, 518
- McClintock J. E., et al., 2011, *Classical and Quantum Gravity*, 28, 114009
- McKinney J. C., Tchekhovskoy A., Blandford R. D., 2012, *ArXiv e-prints*,
- McNamara B. R., Kazemzadeh F., Rafferty D. A., Bîrzan L., Nulsen P. E. J., Kirkpatrick C. C., Wise M. W., 2009, *ApJ*, 698, 594
- Merloni A., Heinz S., 2007, *MNRAS*, 381, 589
- Merloni A., Fabian A. C., Ross R. R., 2000, *MNRAS*, 313, 193
- Meyer-Hofmeister E., Liu B. F., Meyer F., 2009, *A&A*, 508, 329
- Meyer-Hofmeister E., Liu B. F., Meyer F., 2012, *A&A*, 544, A87
- Miller J. M., 2007, *ARA&A*, 45, 441
- Miller M. C., Colbert E. J. M., 2004, *International Journal of Modern Physics D*, 13, 1
- Miller J. M., Homan J., 2005, *ApJ*, 618, L107
- Miller-Jones J. C. A., Jonker P. G., Dhawan V., Briskin W., Rupen M. P., Nelemans G., Gallo E., 2009, *ApJ*, 706, L230
- Miller J. M., et al., 2002, *ApJ*, 570, L69
- Miller J. M., Raymond J., Fabian A., Steeghs D., Homan J., Reynolds C., van der Klis M., Wijnands R., 2006a, *Nat*, 441, 953
- Miller J. M., et al., 2006b, *ApJ*, 646, 394
- Miller J. M., Raymond J., Reynolds C. S., Fabian A. C., Kallman T. R., Homan J., 2008, *ApJ*, 680, 1359
- Miller J. M., Reynolds C. S., Fabian A. C., Miniutti G., Gallo L. C., 2009, *ApJ*, 697, 900
- Miller J. M., Miller M. C., Reynolds C. S., 2011, *ApJ*, 731, L5+
- Mineshige S., Takeuchi M., Nishimori H., 1994, *ApJ*, 435, L125
- Miyamoto S., Kitamoto S., Iga S., Negoro H., Terada K., 1992, *ApJ*, 391, L21
- Morgan C. W., Kochanek C. S., Dai X., Morgan N. D., Falco E. E., 2008, *ApJ*, 689, 755
- Mosquera A. M., Kochanek C. S., Chen B., Dai X., Blackburne J. A., Chartas G., 2013, *ArXiv e-prints*,
- Namiki M., Kawai N., Kotani T., Makishima K., 2003, *PASJ*, 55, 281
- Narayan R., McClintock J. E., 2012, *MNRAS*, 419, L69
- Narayan R., Yi I., 1994, *ApJ*, 428, L13
- Nayakshin S., Kallman T. R., 2001, *ApJ*, 546, 406
- Negoro H., Miyamoto S., Kitamoto S., 1994, *ApJ*, 423, L127
- Negoro H., Kitamoto S., Takeuchi M., Mineshige S., 1995, *ApJ*, 452, L49
- Neilsen J., Lee J. C., 2009, *Nat*, 458, 481
- Neilsen J., Remillard R. A., Lee J. C., 2011, *ApJ*, 737, 69
- Noble S. C., Krolik J. H., Hawley J. F., 2009, *ApJ*, 692, 411
- Noda H., Makishima K., Uehara Y., Yamada S., Nakazawa K., 2011a, *PASJ*, 63, 449

- Noda H., Makishima K., Yamada S., Torii S., Sakurai S., Nakazawa K., 2011b, PASJ, 63, 925
- Nomura M., Ohsuga K., Wada K., Susa H., Misawa T., 2013, PASJ, 65, 40
- Nowak M. A., Wilms J., Dove J. B., 1999, ApJ, 517, 355
- O'Neill S. M., Reynolds C. S., Miller M. C., Sorathia K. A., 2011, ApJ, 736, 107
- Ohsuga K., Mineshige S., 2011, ApJ, 736, 2
- Ohsuga K., Mori M., Nakamoto T., Mineshige S., 2005, ApJ, 628, 368
- Ohsuga K., Mineshige S., Mori M., Kato Y., 2009, PASJ, 61, L7
- Pakull M. W., Mirioni L., 2002, ArXiv Astrophysics e-prints,
- Papitto A., Di Salvo T., D'Ai A., Iaria R., Burderi L., Riggio A., Menna M. T., Robba N. R., 2009, A&A, 493, L39
- Pereyra N. A., Kallman T. R., Blondin J. M., 2000, ApJ, 532, 563
- Ponti G., Fender R. P., Begelman M. C., Dunn R. J. H., Neilsen J., Coriat M., 2012, MNRAS, 422, L11
- Pottschmidt K., et al., 2003, A&A, 407, 1039
- Poutanen J., 2001, Advances in Space Research, 28, 267
- Proga D., 2003, ApJ, 585, 406
- Proga D., Kallman T. R., 2002, ApJ, 565, 455
- Proga D., Stone J. M., Kallman T. R., 2000, ApJ, 543, 686
- Quataert E., Gruzinov A., 2000, ApJ, 539, 809
- Reis R. C., Fabian A. C., Ross R. R., Miniutti G., Miller J. M., Reynolds C., 2008, MNRAS, 387, 1489
- Reis R. C., Miller J. M., Fabian A. C., 2009a, MNRAS, 395, L52
- Reis R. C., Fabian A. C., Ross R. R., Miller J. M., 2009b, MNRAS, 395, 1257
- Reis R. C., Fabian A. C., Miller J. M., 2010, MNRAS, 402, 836
- Reis R. C., et al., 2011, MNRAS, 410, 2497
- Reis R. C., Miller J. M., Reynolds M. T., Gültekin K., Maitra D., King A. L., Strohmayer T. E., 2012a, Science, 337, 949
- Reis R. C., Miller J. M., Reynolds M. T., Fabian A. C., Walton D. J., 2012b, ApJ, 751, 34
- Reynolds C. S., Fabian A. C., 2008, ApJ, 675, 1048
- Reynolds C. S., Nowak M. A., 2003, Phys. Rep. , 377, 389
- Rodriguez J., Corbel S., Hannikainen D. C., Belloni T., Paizis A., Vilhu O., 2004, ApJ, 615, 416
- Ross R. R., Fabian A. C., 2007, MNRAS, 381, 1697
- Russell D. M., Miller-Jones J. C. A., Maccarone T. J., Yang Y. J., Fender R. P., Lewis F., 2011, ApJ, 739, L19
- Russell D. M., Gallo E., Fender R. P., 2013, ArXiv e-prints,
- Schartel N., 2011, Astronomische Nachrichten, 332, 323
- Schnittman J. D., Krolik J. H., 2009, ApJ, 701, 1175
- Schnittman J. D., Homan J., Miller J. M., 2006, ApJ, 642, 420
- Schnittman J. D., Krolik J. H., Noble S. C., 2012, ArXiv e-prints,
- Shafee R., McClintock J. E., Narayan R., Davis S. W., Li L., Remillard R. A., 2006, ApJ, 636, L113
- Shafee R., McKinney J. C., Narayan R., Tchekhovskoy A., Gammie C. F., McClintock J. E., 2008, ApJ, 687, L25
- Shakura N. I., Sunyaev R. A., 1973, A&A, 24, 337
- Shidatsu M., et al., 2011, PASJ, 63, 785
- Shimura T., Takahara F., 1995, ApJ, 445, 780
- Sidoli L., Oosterbroek T., Parmar A. N., Lumb D., Erd C., 2001, A&A, 379, 540
- Sidoli L., Parmar A. N., Oosterbroek T., Lumb D., 2002, A&A, 385, 940
- Sikora M., Begelman M. C., 2013, ApJ, 764, L24
- Sobolewska M. A., Życki P. T., 2006, MNRAS, 370, 405
- Steiner J. F., et al., 2011, MNRAS, pp 1036–+
- Steiner J. F., McClintock J. E., Narayan R., 2013, ApJ, 762, 104
- Stella L., Vietri M., 1998, ApJ, 492, L59
- Strohmayer T. E., Mushotzky R. F., 2003, ApJ, 586, L61
- Strohmayer T. E., Mushotzky R. F., 2009, ApJ, 703, 1386
- Sutton A. D., Roberts T. P., Walton D. J., Gladstone J. C., Scott A. E., 2012, MNRAS, 423, 1154
- Taam R. E., Liu B. F., Meyer F., Meyer-Hofmeister E., 2008, ApJ, 688, 527
- Takahashi H., et al., 2008, PASJ, 60, 69
- Takahashi T., et al., 2012, in Society of Photo-Optical Instrumentation Engineers (SPIE) Conference Series. , arXiv:1210.4378, doi:10.1117/12.926190
- Takeuchi S., Ohsuga K., Mineshige S., 2010, PASJ, 62, L43
- Takeuchi S., Ohsuga K., Mineshige S., 2013, PASJ, 65, 88
- Tanaka Y., et al., 1995, Nat, 375, 659
- Tombesi F., Cappi M., Reeves J. N., Palumbo G. G. C., Yaqoob T., Braitto V., Dadina M., 2010a, A&A, 521, A57
- Tombesi F., Sambruna R. M., Reeves J. N., Braitto V., Ballo L., Gofford J., Cappi M., Mushotzky R. F., 2010b, ApJ, 719, 700
- Tomsick J. A., Yamaoka K., Corbel S., Kaaret P., Kalemci E., Migliari S., 2009, ApJ, 707, L87

- Torii S., et al., 2011, PASJ, 63, 771
- Turner M. J. L., et al., 1989, PASJ, 41, 345
- Ueda Y., Inoue H., Tanaka Y., Ebisawa K., Nagase F., Kotani T., Gehrels N., 1998, ApJ, 492, 782
- Ueda Y., Asai K., Yamaoka K., Dotani T., Inoue H., 2001, ApJ, 556, L87
- Ueda Y., Murakami H., Yamaoka K., Dotani T., Ebisawa K., 2004, ApJ, 609, 325
- Ueda Y., Yamaoka K., Remillard R., 2009, ApJ, 695, 888
- Vaughan S., Fabian A. C., 2004, MNRAS, 348, 1415
- Vierdayanti K., Mineshige S., Ebisawa K., Kawaguchi T., 2006a, PASJ, 58, 915
- Vierdayanti K., Mineshige S., Ebisawa K., Kawaguchi T., 2006b, PASJ, 58, 915
- Vierdayanti K., Done C., Roberts T. P., Mineshige S., 2010, MNRAS, 403, 1206
- Volonteri M., Sikora M., Lasota J.-P., Merloni A., 2013, ApJ, 775, 94
- Walton D. J., Roberts T. P., Mateos S., Heard V., 2011, MNRAS, 416, 1844
- Walton D. J., Miller J. M., Reis R. C., Fabian A. C., 2012, MNRAS, 426, 473
- Watarai K.-y., Mizuno T., Mineshige S., 2001, ApJ, 549, L77
- Webb N. A., Barret D., Godet O., Servillat M., Farrell S. A., Oates S. R., 2010, ApJ, 712, L107
- Wilkins D. R., Fabian A. C., 2012, MNRAS, 424, 1284
- Wilkinson T., Uttley P., 2009, MNRAS, 397, 666
- Woods D. T., Klein R. I., Castor J. I., McKee C. F., Bell J. B., 1996, ApJ, 461, 767
- Yamada S., Negoro H., Torii S., Noda H., Mineshige S., Makishima K., 2013, ApJ, 767, L34
- Yamaoka K., Ueda Y., Inoue H., Nagase F., Ebisawa K., Kotani T., Tanaka Y., Zhang S. N., 2001, PASJ, 53, 179
- Yamauchi S., Kawai N., Aoki T., 1994, PASJ, 46, L109
- Yoshida T., Isobe N., Mineshige S., Kubota A., Mizuno T., Saitou K., 2013, PASJ, 65, 48
- Zdziarski A. A., Sikora M., Dubus G., Yuan F., Cerutti B., Ogorzałek A., 2012, MNRAS, 421, 2956
- Zoghbi A., Fabian A. C., Reynolds C. S., Cackett E. M., 2012, MNRAS, 422, 129
- van der Klis M., 2006, Rapid X-ray Variability. pp 39–112